Potassium Amphibole Stability in the Upper Mantle: an Experimental Study in a Peralkaline KNCMASH System to 8.5 GPa

Originally published in:
Journal of Petrology 38(5), https://doi.org/10.1093/petroj/38.5.537

JOURNAL OF PETROLOGY | VOLUME 38 | NUMBER 5 | PAGES 537–568 | 1997

Potassium Amphibole Stability in the Upper Mantle: an Experimental Study in a Peralkaline KNCMASH System to 8·5 GPa

J. KONZETT*, R. J. SWEENEY, A. B. THOMPSON AND P. ULMER

INSTITUT FÜR MINERALOGIE UND PETROGRAPHIE, ETH-ZENTRUM, SONNEGGSTR. 5, CH-8092 ZÜRICH, SWITZERLAND

RECEIVED JUNE 12, 1996 ACCEPTED NOVEMBER 21, 1996

Experiments were performed from 1·0 to 8·5 GPa in a peralkaline system K_2O–Na_2O–CaO–MgO–Al_2O_3–SiO_2–H_2O (KNCMASH) to investigate the stability and composition of richteritic amphiboles in the MARID (mica–amphibole–rutile–ilmenite–diopside) assemblage amphibole + phlogopite + clinopyroxene. The results were compared with phase relations and the composition of natural MARIDs to assess possible mechanisms of formation for MARID-type rocks. K-richterite is stable in a wide range of bulk K/Na ratios in the MARID assemblage to 8·5 GPa and 1300°C. In this assemblage the amphibole can accommodate significant amounts of K on the M(4)-site and shows a systematic increase in the K/Na ratio with increasing pressure. At P *>7·0 GPa, K-richterite can coexist with garnet. Phase relations of K-richterite in a natural MARID composition are consistent with those in the simplified system and confirm the potential stability of K-richterite and K-richterite + garnet within the diamond stability field. The assemblage K-richterite + phlogopite + clinopyroxene is incompletely buffered in the KNCMASH system, resulting in a systematic relation between bulk- and mineral compositions observed in the experiments. Such a correlation, however, cannot be observed in natural MARIDs. Therefore, MARID-type rocks do not represent the bulk composition from which they formed and, hence, must be products of an open-system crystallization.*

KEY WORDS: *K-richterite; high-*P *experiments; MARID xenoliths; mantle metasomatism*

INTRODUCTION

K-rich amphiboles are exotic members of the amphibole family in terms of their frequency of occurrence at the Earth's surface. With few exceptions they are represented by K-rich varieties of richterite $NaCaNaMg_5Si_8O_{22}(OH)_2$, katophorite $NaCaNaMg_4AlSi_7AlO_{22}(OH)_2$ and, more rarely, arfvedsonite $NaNa_2Mg_4Fe^{3+}Si_8O_{22}(OH)_2$. The vast majority of known occurrences is confined to extremely alkaline, K-dominated mainly magmatic environments which are poor in Al and partly Si undersaturated. Experimental results on K-richterite stability show that this amphibole can act as a principal reservoir for alkalis and water as well as for a number of incompatible trace elements in the Earth's mantle down to transition zone depths, and may be involved in deep-seated magma generation processes: K-richterite (or Ti- and/or F-rich varieties) is thought to be a source component of lamproites and group II kimberlites (orangeites) (Foley, 1992; Taylor *et al.*, 1994; Mitchell, 1995*b*).

Previous studies have dealt with K-richterite stability in various bulk systems and little attention has been given so far to K-richterite chemistry as a function of *P*, *T* and bulk chemistry of the mantle. Thus, the aims of the present study are twofold: first, to assess the stability of K-richterite as a function of *P* and *T* in a peralkaline bulk composition; second, to consider the dependence of the chemistry of amphibole and coexisting clinopyroxene and phlogopite upon changing bulk composition.

*Corresponding author. Telephone: (41-1) 01 632 3803. Fax: (41-1) 01 632 1088. e-mail: juergen@erdw.ethz.ch

OCCURRENCE OF POTASSIC AMPHIBOLES

There are two typical occurrences of K-rich amphiboles: the first is in ultrabasic xenoliths from kimberlites and the second is in lamproites. In ultrabasic xenoliths they appear in usually phlogopite-dominated MARID (mica–amphibole–rutile–ilmenite–diopside) xenoliths (Dawson & Smith, 1977) as well as in phlogopite-bearing lherzolites and harzburgites, termed the PKP (phlogopite–K-richterite peridotite) peridotite suite (Erlank *et al.*, 1987). K-rich amphiboles from kimberlitic xenoliths show a restricted range in composition and closely approach the formula of K-richterite, $KNaCaMg_5Si_8O_{22}(OH)_2$, with only minor amounts of Fe and negligible Al, Ti, Cr and F (Erlank & Finger, 1970; Aoki, 1975; Dawson & Smith, 1977; Jones *et al.*, 1982; Erlank *et al.*, 1987). Compared with PKPs, K-richterites from MARIDs are higher in Fe and Ti, and lower in Cr and Mg (Jones *et al.*, 1982; Erlank *et al.*, 1987). K-richterites are believed to have formed by metasomatism of the upper mantle before entrainment of the xenoliths into the host kimberlites (Dawson & Smith, 1977; Waters, 1987*a*; Erlank *et al.*, 1987).

Lamproitic amphiboles (Mitchell & Bergman, 1991) are typically rich in Ti (up to ~8 wt % TiO_2) compared with K-richterites from kimberlitic xenoliths, and exhibit a wider compositional range mainly comprising titanian K-richterites and titanian K-magnesio-katophorites. Textures (Mitchell & Bergman, 1991; Hwang *et al.*, 1994) as well as experimental work (Barton & Hamilton, 1982; Edgar *et al.*, 1992; Mitchell, 1995*a*) suggest lamproitic amphiboles to be late crystallizing near-solidus or subsolidus phases.

Apart from these typical occurrences, K-rich amphiboles have been occasionally encountered in a number of alkaline rocks: as xenocrysts or within xenoliths from alkaline lamprophyres and olivine nephelinites (Wagner *et al.*, 1995, 1996), or as a groundmass phase from minettes (Hall, 1982; Nemec, 1988), leucite-bearing lavas (Cundari, 1973) and certain group II kimberlites (Mitchell, 1995*b*). K-richterite associated with phlogopite has also been described as an inclusion in diamond from the Sloan kimberlite, Colorado (Meyer & McCallum, 1986) and associated with clinopyroxene inclusions in diamond from Fuxian (Leung *et al.*, 1994). K-rich amphiboles of crustal origin seem to be extremely rare: K-richterite has been reported from contact-metamorphic metacherts (Heinrich, 1994), contact-metamorphic volcanic ejecta (Della Ventura *et al.*, 1983) and in blueschist-facies manganese schists (Mottana & Griffin, 1986). Occurrences of potassium pargasites have been reported by Shimazaki *et al.* (1984) and Matsubara & Motoyoshi (1985) from granulite facies skarns.

SYNTHESIS AND STABILITY OF K-RICHTERITE

K-richterite was first synthesized by Hübner & Papike (1970) at low pressures for crystal chemical studies. These workers noted that the potassic amphibole had a smaller molar volume than the chemically equivalent phlogopite + diopside, and thus concluded it should be stable at higher pressures than mica + pyroxene. The first high-pressure experiments to constrain the stability field of K-richterite were performed by Kushiro & Erlank (1970), who found natural K-richterite to be stable up to 3 GPa and 1100°C on its own, and up to 2·4 GPa and 1000°C in the presence of clinopyroxene. Gilbert & Briggs (1974) determined the high-temperature stability limit of synthetic K-richterite and located the amphibole breakdown curve up to 2·5 GPa and >1200°C with a positive slope of the reaction over the whole investigated P–T range. On the other hand, Hariya & Terada (1973) proposed a K-richterite stability field similar in shape to that of pargasite with a backbend of the K-richterite-out reaction and an (extrapolated) upper P stability limit of ~3·5 GPa. This suggestion was disproved by Foley (1991), who determined the upper temperature stability limit up to 5 GPa of synthetic K-and K-fluorine-richterite with positive dP/dT. An extension of experiments to P >5 GPa by Trønnes *et al.* (1988) showed that end-member K-richterite is stable at 10 GPa to temperatures as high as 1450°C and has an upper pressure stability limit between 14 and 15 GPa, where it breaks down to diopside + clinoenstatite + stishovite + fluid. Trønnes *et al.* (1988) also observed growth of K-richterite + garnet at 10 GPa at the expense of phlogopite in natural phlogopite-doped peridotite. In an Na-free system, Sudo & Tatsumi (1990) stabilized KKCa-richterite with garnet from a diopside + phlogopite mixture between 6 and 7 GPa at 1100°C.

COMPOSITION AND PREPARATION OF STARTING MATERIALS

A simplified MARID-like bulk system K_2O–Na_2O–CaO–MgO–Al_2O_3–SiO_2–H_2O (KNCMASH) has been chosen for the following reasons: (1) K-richterite, phlogopite and clinopyroxene in MARIDs are sufficiently low in both Fe and Ti (see Erlank *et al.*, 1987) to be adequately represented by KNCMASH; (2) (Fe)Ti phases usually make up <5 vol. % of MARID xenoliths (Waters, 1987*b*). Omission of Fe avoids oxidation problems and allows unambiguous recalculation of mineral formulae. Inclusion of Na is critical in understanding the effect of omphacitic pyroxene on the stability of K-amphibole and mica with garnet in KNCMASH.

Four different bulk compositions were prepared for experiments in the KNCMASH system. Experimental

bulk composition 1 was used to delimit the K-richterite stability field. This composition was prepared to contain more $K_2O + Na_2O$ than natural MARID AJE137 used by Sweeney *et al.* (1993) in their experiments to 3·5 GPa (Table 1) to compensate for a possible loss of alkalis from the solid bulk to the fluid at very high pressures. The compositions 2, 3 and 4 were prepared to investigate the effect of changing K/Na on the phase relations. Experimental bulk compositions are plotted on the Al_2O_3–($K_2O + Na_2O$)–olivine face of a tetrahedron with Al_2O_3–($K_2O + Na_2O$)–SiO_2–olivine apices as shown in Fig. 1 (see Sweeney *et al.*, 1993). Despite a considerable range in Al contents and K/Na ratios (Waters, 1987*a*), MARIDs as well as clinopyroxene-absent MARIs are peralkaline, because all typical MARI(D) mineral phases have molar $(K_2O + Na_2O)/Al_2O_3 \geq 1$ with bulk values ranging from 1·1 to 5·9. The starting material for the present study has a molar $(K_2O + Na_2O)/Al_2O_3$ of 1·72. Amphibole-absent but still clinopyroxene-containing mica–rutile–ilmenite–diopside (MRIDs) xenoliths and K-richterite-bearing metasomatized peridotites (PKPs) straddle the olivine–$(K,Na)_2Al_2O_4$ join but are usually still peralkaline. For comparison with the experimental compositions, an average of six MARID bulk compositions, an average of 11 MARI(D) bulk compositions (Waters, 1987*a*), an average PKP composition (Erlank *et al.*, 1987) as well as the composition of AJE137 used by Sweeney *et al.* (1993) are given in Table 1. Natural MARI(D)s contain between 1·5 and 4 wt % H_2O [equivalent to loss on ignition (LOI); Waters, 1987*a*]. To ensure water-excess subsolidus conditions, 5 wt % H_2O were added to the starting material in this study.

Mixtures of synthetic oxides and carbonates were used as a starting material with H_2O added to the anhydrous oxide mixture as brucite. SiO_2, MgO and Al_2O_3 were fired at 1200°C for 12 h; K_2CO_3, $CaCO_3$, Na_2SiO_3 and $Mg(OH)_2$ were dried at 220°C for 12 h. Mixtures of SiO_2, MgO, Al_2O_3, K_2CO_3 and $CaCO_3$ in the desired proportions were homogenized and put into Pt crucibles. After pre-heating to 250°C for 15 min the mixtures were fired at 700°C for 15 h. The temperature was then increased to 1100°C in 50°C intervals with intermittent checks of LOI. In a final step, Na_2SiO_3 and $Mg(OH)_2$ were added to the fired oxide mixtures in the desired proportions; 2–3 mg of these mixtures were loaded in Pt_{100} capsules of 1·6 mm diameter and welded shut.

EXPERIMENTAL AND ANALYTICAL TECHNIQUES

Experiments from 1·0 to 3·0 GPa were conducted with a non-endloaded and an endloaded piston cylinder with 14 and 22 mm bore, respectively. All experiments at pressure >3·0 GPa were performed in a Walker-type two-stage 6/8 multi-anvil module (Walker *et al.*, 1990; Walker, 1991) in a 1000-ton press.

Piston cylinder apparatus

NaCl and NaCl–Pyrex assemblies were used to the highest temperatures. Temperatures were measured with $Pt–Pt_{90}Rh_{10}$ and chromel–alumel (type K) thermocouples and are considered accurate to ± 5°C, without taking into account the effect of pressure on e.m.f. Pressure was calibrated at 600°C against the reaction albite = jadeite + quartz (1·61 GPa; Johannes *et al.*, 1971), and at 1000°C against the reactions fayalite + quartz = orthoferrosilite (1·41 GPa; Bohlen *et al.*, 1980) and quartz = coesite (3·07 GPa; Bose & Ganguly, 1995). Pressures are considered accurate to $\pm 0·05$ GPa.

Multi-anvil apparatus

The experiments (Table 2) were performed with WC cubes with a truncated edge length (TEL) of 12 mm. The pressure-transmitting octahedron and gasket-fins are fabricated from MgO-based castable ceramic. All runs (including high-temperature calibration experiments) were performed with 3·5 mm outside diameter stepped graphite furnace assemblies. The temperatures were measured with one thermocouple at the bottom of the capsule and in some experiments with a second thermocouple attached to the capsule wall (Fig. 2). This arrangement showed that thermal gradients at 1200°C do not exceed ~30°C/mm (Fig. 2). The vertical length of the charge in individual capsules ranges between ~1·5 and 2·0 mm. High-temperature calibration experiments were performed on the following phase transitions: quartz–coesite (3·2 GPa at 1200°C; Bose & Ganguly, 1995), fayalite–γ-Fe_2SiO_4 (5·0 GPa at 1000°C; Yagi *et al.*, 1987), $CaGeO_3$ garnet–perovskite transition (6·1 GPa at 1000°C; Susaki *et al.*, 1985) and coesite–stishovite (9·1 GPa at 1000°C; Yagi & Akimoto, 1976). Pressures and temperatures are considered to be accurate to $\pm 0·2$ GPa and ± 15°C, respectively. All temperatures quoted are thermocouple readings from the Eurotherm controller, not corrected for the pressure effect on e.m.f. During the runs, temperatures were kept constant to within ± 2°C and the applied load to within ± 1 ton (strain-gauge reading; corresponding to $\leq 0·02$ GPa) and recorded during the entire duration of the experiment.

Analytical technique

After each experiment, capsules were embedded longitudinally in epoxy resin and ground to expose the centre of the charge. During opening, small amounts of water extruded from the capsules. This was taken as an

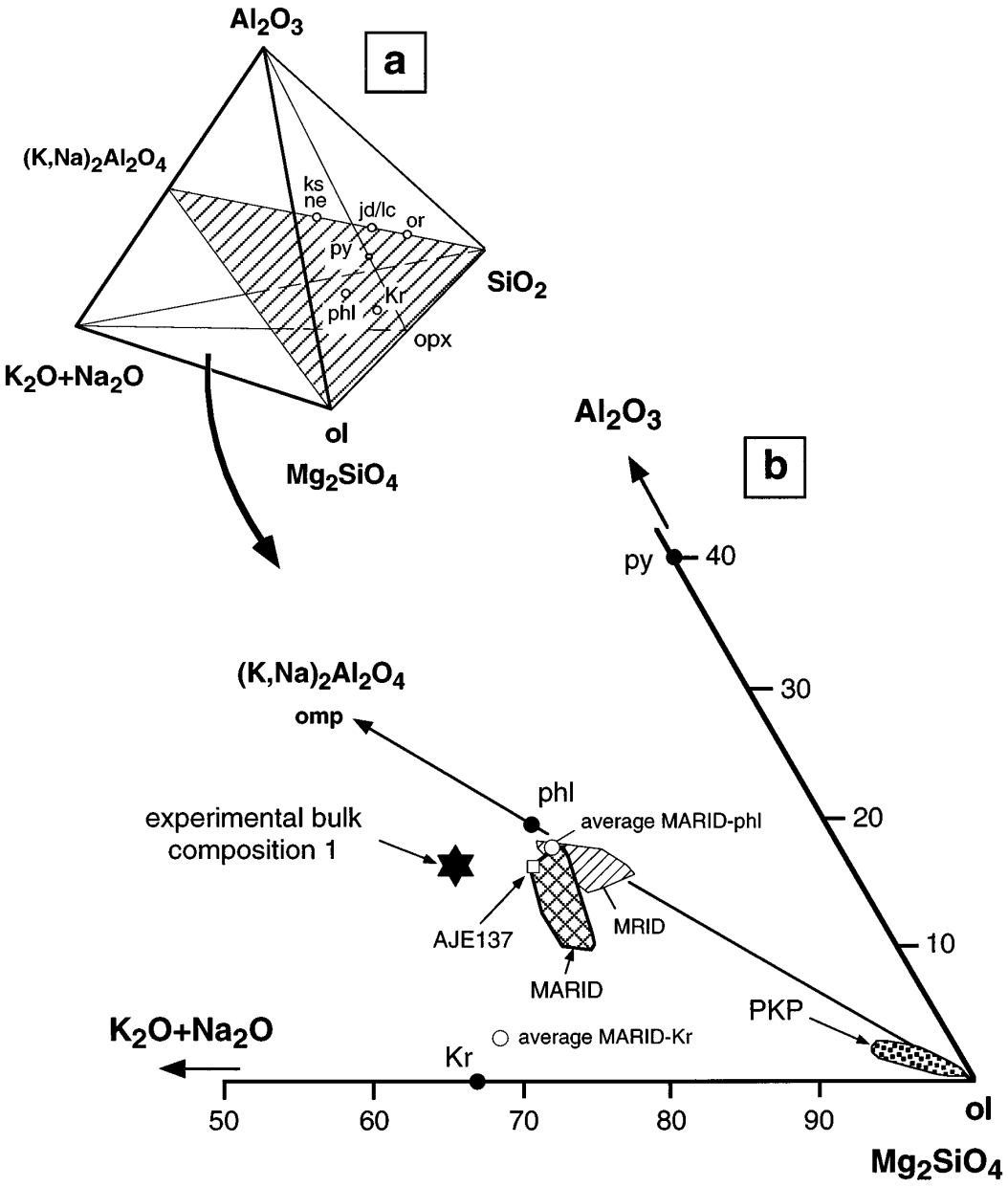

Fig. 1. (a) KNMAS molecular tetrahedron and (b) a projection onto the Al_2O_3–(Na_2O + K_2O)–Mg_2SiO_4 plane of the KNMAS tetrahedron from the SiO_2 apex (Sweeney *et al.*, 1993). For Ca-bearing compositions diopside saturation is assumed and subtracted before projection. (a) The shaded plane divides the tetrahedron into two regions: compositions with molar (K_2O + Na_2O)/Al_2O_3 <1 (i.e. subalkaline compositions) plot above the plane, those with (K_2O + Na_2O)/Al_2O_3 >1 (i.e. peralkaline compositions) below the plane. (b) The star denotes experimental bulk compositions 1–4. ●, compositions of pure K-richterite $KNaCaMg_5Si_8O_{22}(OH)_2$, phlogopite $KMg_3AlSi_3O_{10}(OH)_2$ and pyrope $Mg_3Al_2Si_3O_{12}$. ○, compositions of average natural MARID K-richterite and phlogopite as given by Erlank *et al.* (1987). Shaded areas: compositional range of MARID (mica–amphibole–rutile–ilmenite–phlogopite), MRID (mica–rutile–ilmenite–diopside) xenoliths (Waters, 1987*a*) and PKP (phlogopite–K-richterite peridotite) xenoliths (Erlank *et al.*, 1987). Abbreviations: jd, jadeite; Kr, K-richterite; ks, kalsilite; lc, leucite; ne, nepheline; opx, orthopyroxene; or, orthoclase; phl, phlogopite; py, pyrope.

indication of water-saturated conditions at subsolidus temperatures and of integrity of the capsule during the run. Accurate determination of the weight loss was not possible owing to assembly material adhering to the capsule.

Run products were first inspected using a reflected

Table 1: Composition of synthetic and natural starting materials used in the present study compared with compositions of natural MARIDs and PKPs

	Exp. bulk 1	Exp. bulk 2	Exp. bulk 3	Exp. bulk 4	AJE 137	Average MARID	Average MARI(D)	Average PKP
wt %								
SiO_2	47·61	47·15	47·75	47·08	45·57	45·45 ± 1·64	44·70 ± 1·84	42·66
TiO_2	—	—	—	—	3·03	2·67 ± 0·42	3·55 ± 2·50	0·22
Al_2O_3	6·67	6·67	6·69	6·20	6·55	6·34 ± 1·88	6·00 ± 2·82	0·85
Cr_2O_3	—	—	—	—	0·15	0·19 ± 0·13	0·19 ± 0·10	0·28
Fe_2O_3	—	—	—	—	7·53	7·24 ± 0·37	7·50 ± 1·44	7·93
MnO	—	—	—	—	0·06	0·07 ± 0·01	0·07 ± 0·02	0·11
MgO	23·79	23·67	23·71	23·87	21·08	21·58 ± 1·26	21·94 ± 1·54	40·14
CaO	7·61	7·99	7·67	7·60	5·74	5·67 ± 1·93	4·81 ± 2·20	1·12
Na_2O	1·94	3·11	3·72	0·33	0·91	0·92 ± 0·46	1·06 ± 0·64	0·23
K_2O	7·62	6·70	5·77	10·15	6·95	6·91 ± 1·25	6·91 ± 1·86	0·93
P_2O_5	—	—	—	—	0·07	0·06 ± 0·03	0·05 ± 0·03	0·05
NiO	—	—	—	—	0·08	0·08 ± 0·03	0·20 ± 0·30	0·26
LOI	—	—	—	—	3·09	2·47 ± 1·40	2·65 ± 1·12	5·05
H_2O	4·76	4·71	4·69	4·77	—		—	—
Total	100·00	100·00	100·00	100·00	100·81	99·64 ± 1·63	99·63 ± 1·58	99·83
PI	1·72	1·85	1·85	1·86	1·38	1·50 ± 0·36	2·19 ± 1·73	1·63
K/Na	2·58	1·42	1·02	20·34	5·03	7·21 ± 6·45	7·18 ± 6·56	2·66

exp. bulk 1, 2, 3, 4, composition of starting materials for the present study; AJE137, natural MARID composition (Waters, 1987*a*) used for experiments by Sweeney *et al.* (1993); average MARID, average of six bulk analyses of MARIDs (Waters, 1987*a*; table 3, analyses 1–6); average MARI(D): average of 11 bulk analyses of MARIDs and cpx-free MARIs (Waters 1987*a*, table 3, analyses 1–11); average PKP, average of 31 bulk analyses of phlogopite–K-richterite peridotites (PKPs) given by Erlank *et al.* (1987) (table IVd); PI (peralkalinity index) = molar $(K_2O + Na_2O)/Al_2O_3$.

light microscope and subsequently analysed with a Cameca Sx50 electron microprobe equipped with five wavelength-dispersive spectrometers. Natural and synthetic oxides and silicates were used as standards. The raw data were corrected on-line with the PAP correction procedure. Analytical conditions were 15 kV acceleration voltage and 20 nA sample current. Beam size was minimized (~1 μm) for most analyses. Dependent on the grain size of individual phases, 3–19 grains of each phase were measured from each experiment.

Recalculation of mineral formulae

K-richterite analyses were recalculated assuming 23 oxygens and stoichiometric OH. In this case cation sums are usually very close to 16·00. Owing to uncertainty of individual microprobe analyses, cation sums up to 16·03 were accepted as representative. Cations were assigned to structural positions as follows: (a) T-sites: all Si, then sufficient Al to sum to 8·0; (b) M(1)–M(2)–M(3)-sites: remaining Al, then Mg to sum to 5·0; (c) M(4): remaining Mg, then Ca and Na to sum to 2·0; (d) A-site: remaining Na and K. In the case of Σ(Mg + Ca + Na) on M(4) <2·0, K was assigned to M(4). This is crystallographically reasonable, as discussed below. Phlogopites were recalculated assuming 11 oxygens and stoichiometric OH, clinopyroxenes assuming six oxygens and garnets assuming 12 oxygens.

RESULTS OF THE EXPERIMENTS

Petrography

At temperatures $\geq$1100°C individual grains are usually coarse and some are perfectly euhedral. K-richterites form isometric or elongated grains with rounded edges (Fig. 3); the maximum grain size is ~100 μm × 40 μm, and an approximate mean size is 20 μm × 20 μm. Phlogopites in most cases show euhedral rectangular shape with a size distribution comparable with that of amphibole. Clinopyroxenes form somewhat smaller crystals in the range of 5–10 μm, rarely exceeding 20 μm in length; they are often euhedral in shape and tend to form clusters as opposed to amphibole and mica, which normally occur as isolated grains. Garnet always appears as isometric grains (Fig. 3) with sizes exceeding

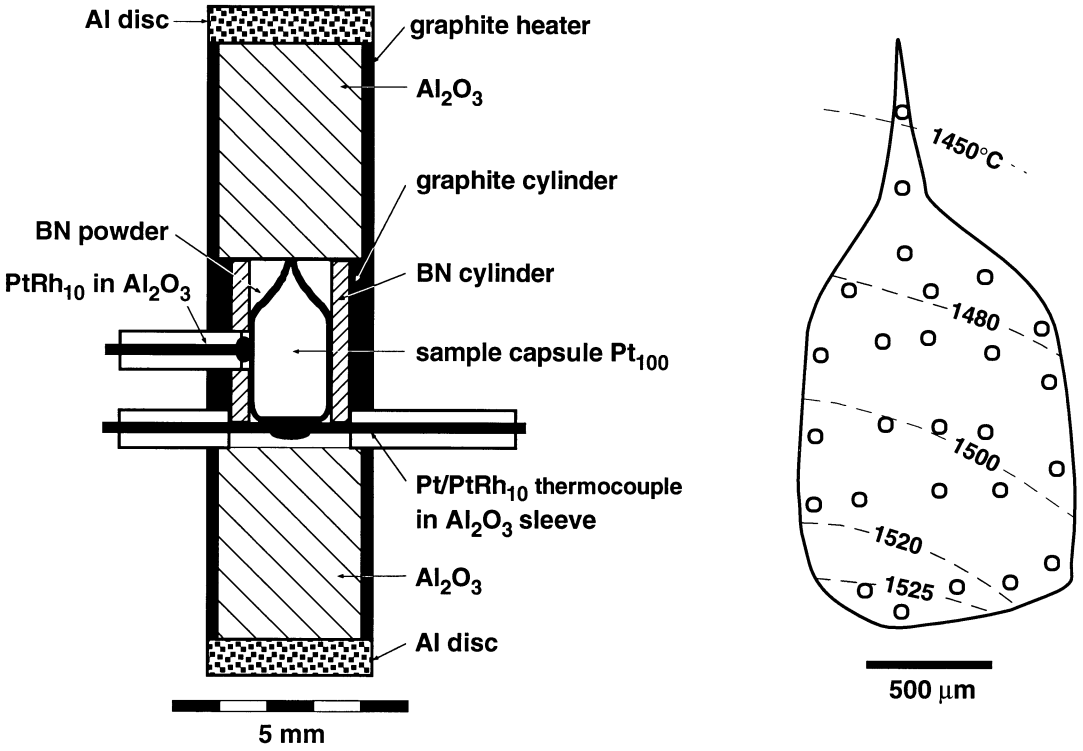

Fig. 2. Sketch of 3·5 mm diameter stepped graphite furnace assemblage (left) and distribution of isotherms in an experimental charge (right) deduced from coexisting clinopyroxene and applying the geothermometer of Brey & Köhler (1990) to a mixture of synthetic $diopside_{30}enstatite_{70}$ + 10% BaB_2O_7 flux (run conditions: 1550°C at 6·0 GPa). ○, positions of analysed coexisting pyroxenes used to constrain the T distribution.

100 μm at 8·0 GPa and 1400°C. Large garnets are in part extremely poikiloblastic with numerous clinopyroxene and/or olivine inclusions. Olivine is present only in trace amounts with a size <10 μm at 1100°C, and often associated with feathery quench-phlogopite. At temperatures above the inferred solidus (1200°C) the grain size of olivine may increase to >20 μm. At temperatures <1000°C the grain size is much smaller and especially clinopyroxene was difficult to analyse, as grains rarely exceed 5 μm in diameter. Experimental results are listed in Table 2 and plotted in Fig. 5 (see below).

Distribution and modal amounts of phases in the charge

The distribution of phases in some experiments is inhomogeneous. Detectable quench-phlogopite is often situated at the bottom of the capsule, even in experiments with temperature gradients <20°C/mm. At 1100°C olivine is concentrated within the quench-zone; at above-solidus conditions olivine is evenly distributed throughout the charge. In run Ma34 with a temperature gradient ≤33°C/mm two different assemblages occur within the capsule. The boundary between the assemblages is consistent with a distribution of isotherms within capsules (Fig. 2).

Modal analyses of runs from 1·5 GPa and 900°C to 8·0 GPa and 1100°C were performed by comparing the experimental bulk composition with a best-fit linear combination of average compositions of the observed phases. Results of this calculation (Fig. 4) show that the bulk lies within the composition space spanned by the assemblage K-richterite + phlogopite + clinopyroxene + H_2O. This occurs despite the expected high solubility of oxides in high-pressure fluids and the presence of some quench in Ma69. Calculated changes in the modal amounts as a function of pressure are small and involve only a slight increase in K-richterite at the expense of phlogopite. Calculated modes were compared with the actual modes obtained by image analysis of nine areas each ~250 μm × 250 μm in size containing several hundred grains. Averaged observed modal amounts of K-richterite are close to the calculated values (Fig. 4), but show a high standard deviation owing to an inhomogeneous distribution ranging from 12 to 35 vol. % for individual areas in Ma69 and from 5 to 27 vol. % in Ma31.

Table 2: Summary of experimental run conditions and products

Exp. no.:	Exp. technique	Starting comp.	*P* (GPa)	*T* (°C) TC_1	*T* (°C) TC_2	Run time (h min)	Phases identified
Ma20	MA	bulk 1	4·0	1250	1223	02h12	phl + cpx + ol + Q
Ma24	MA	bulk 1	8·5	1100	1084	02h10	Kr + phl + cpx + ol + Q
Ma27	MA	bulk 1	7·5	1100	1102	07h10	Kr + phl + cpx + ol + Q
Ma31	MA	bulk 1	4·0	1100	1084	08h02	Kr + phl + cpx + Q
Ma34	MA	bulk 1	4·0	1200	1136	03h04	TC_1: phl + cpx + ol + Q TC_2: phl + cpx + Kr
Ma35	MA	bulk 1	6·0	1100		07h12	Kr + phl + cpx
Ma37	MA	bulk 1	4·0	1000	1005	12h10	Kr + phl + cpx
Ma39	MA	bulk 1	4·0	900	888	27h15	Kr + phl + cpx
Ma42	MA	bulk 1	5·0	1100	1062	08h00	Kr + phl + cpx + Q
Ma51	MA	bulk 1	4·0	800		95h42	Kr + phl + cpx
Ma69	MA	bulk 1	8·0	1100		25h30	Kr + phl + cpx + ol + Q
Ma70	MA	bulk 1	8·0	1300		04h48	Kr + phl + cpx + ga + ol + Q
Ma71	MA	bulk 2	4·0	1100		09h16	Kr + phl + cpx + Q
Ma72	MA	bulk 3	4·0	1100		09h16	Kr + phl + cpx + ol + Q
Ma73	MA	bulk 1	8·0	1200	1161	06h10	Kr + phl + cpx + ol + Q
Ma74	MA	bulk 1	8·0	1400		04h16	cpx + ga + ol + Q
Ma75	MA	bulk 1	6·0	1300	1298	07h04	phl + cpx + ol + Q
Ma77	MA	bulk 1	4·5	1100	1100	25h47	Kr + phl + cpx + Q
Ma78	MA	bulk 1	7·0	1300		04h00	Kr* + phl + cpx + ol + Q
Ma79	MA	bulk 4	4·0	1100		09h10	Kr + phl + cpx
Ma84	MA	bulk 1	7·0	1100		23h42	Kr + phl + cpx + ol + Q
JK12	PC	bulk 1	1·0	900		73h12	phl + cpx
JK16	PC	bulk 1	3·0	1100		99h03	Kr + phl + cpx + Q
JK22	PC	bulk 4	3·0	1000		126h30	Kr + phl + cpx
JK23	PC	bulk 1	3·0	1000		126h30	Kr + phl + cpx
JK25	PC	bulk 1	2·0	900		162h12	Kr + phl + cpx
JK27	PC	bulk 1	1·5	900		172h42	Kr + phl + cpx
ma1	MA	AJE137	4·6	1400		00h30	ol + opx + ga + cpx + Q
ma2	MA	AJE137	4·6	1240		00h48	phl + opx + cpx
ma3	MA	AJE137	6·8	1345		00h20	ol + opx + ga + cpx + Q
ma4	MA	AJE137	7·5	1300		00h42	ol + opx + ga + cpx + Q
ma5	MA	AJE137	7·5	1200		01h10	Kr + phl + cpx + ga + opx
ma6	MA	AJE137	6·0	1200		00h25	opx + cpx + phl + Ti-phase

Kr, K-richterite; phl, phlogopite; cpx, clinopyroxene; opx, orthopyroxene; ga, garnet; ol, olivine; Q, quench fluid/melt.
*Kr is present in the cooler end of the capsule.

Chemical homogeneity of the phases

With the exception of garnet all phases are chemically homogeneous. Large garnets often exhibit diffuse cores which have high Al contents. In most cases, small garnets <10 μm are chemically and optically homogeneous. Al-rich cores are interpreted as remnants of unreacted Al_2O_3 inherited from the starting material, on which garnet preferentially nucleated. The Al-rich cores are overgrown by rims of up to 10 μm width which show constant composition and are thought to represent the equilibrium garnet composition at prevailing *P* and *T*. This indicates that equilibrium was achieved at grain contacts so that the small unreacted cores of the larger garnets are not volumetrically sufficient to cause a significant shift in the bulk composition. No systematic differences in phase chemistries occur between phases analysed from the

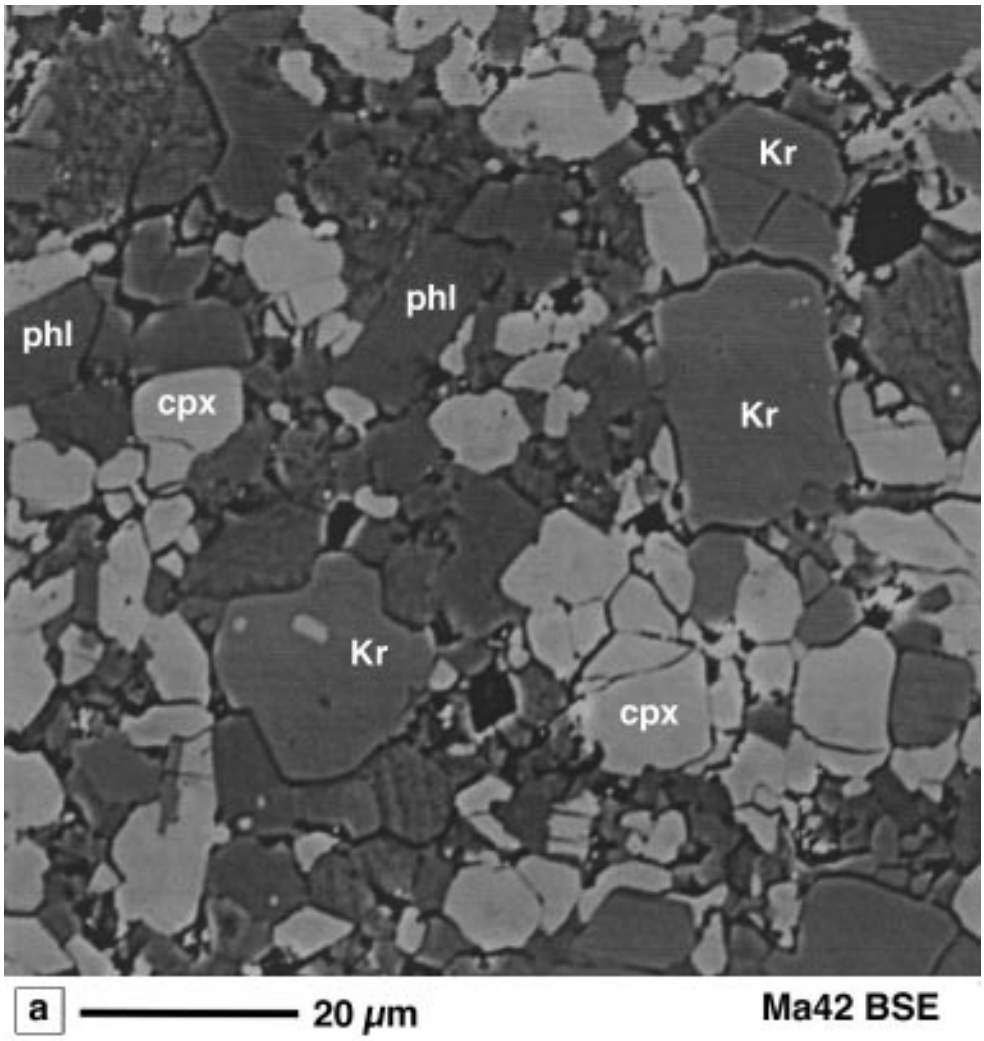

Fig. 3.

bottom or the top of the capsules. This also applies to runs with high T gradients such as Ma34 in which clinopyroxene and phlogopite occur without K-richterite at the hotter capsule-bottom but coexisting with K-richterite at the cooler end of the capsule.

Phase relations in KNCMASH

The location of the solidus

Locating the solidus in alkali and water-rich bulk systems is often hampered by severe problems of melt recognition owing to quench crystallization. Because of the high solubility of alkalis and silica in high-pressure fluids (see, e.g. Ryabchikov & Boettcher, 1980; Schneider & Eggler, 1986) solute-rich quenched vapour at subsolidus conditions cannot unambiguously be optically distinguished from quenched melt. Moreover, the P–T conditions at which melt first becomes visible are not identical to the true solidus P–T conditions because up to ~5 vol. % of melt can remain undetected as grain-boundary films unless investigated by transmission electron microscopy (TEM). Thus, in the present study the inferred temperature of the solidus at 4·0 and 8·0 GPa based on textural observations should be considered a maximum temperature.

Stability of K-richterite

The stability field of K-richterite in the present bulk system may be divided into a lower-T–lower-P region where K-richterite coexists with phlogopite + clinopyroxene ± olivine + vapour (Kr-field I) and a high-T–high-P region (Kr-field II) above 7·0 GPa and 1200°C where K-richterite coexists with garnet in an assemblage K-richterite + phlogopite + clinopyroxene + garnet

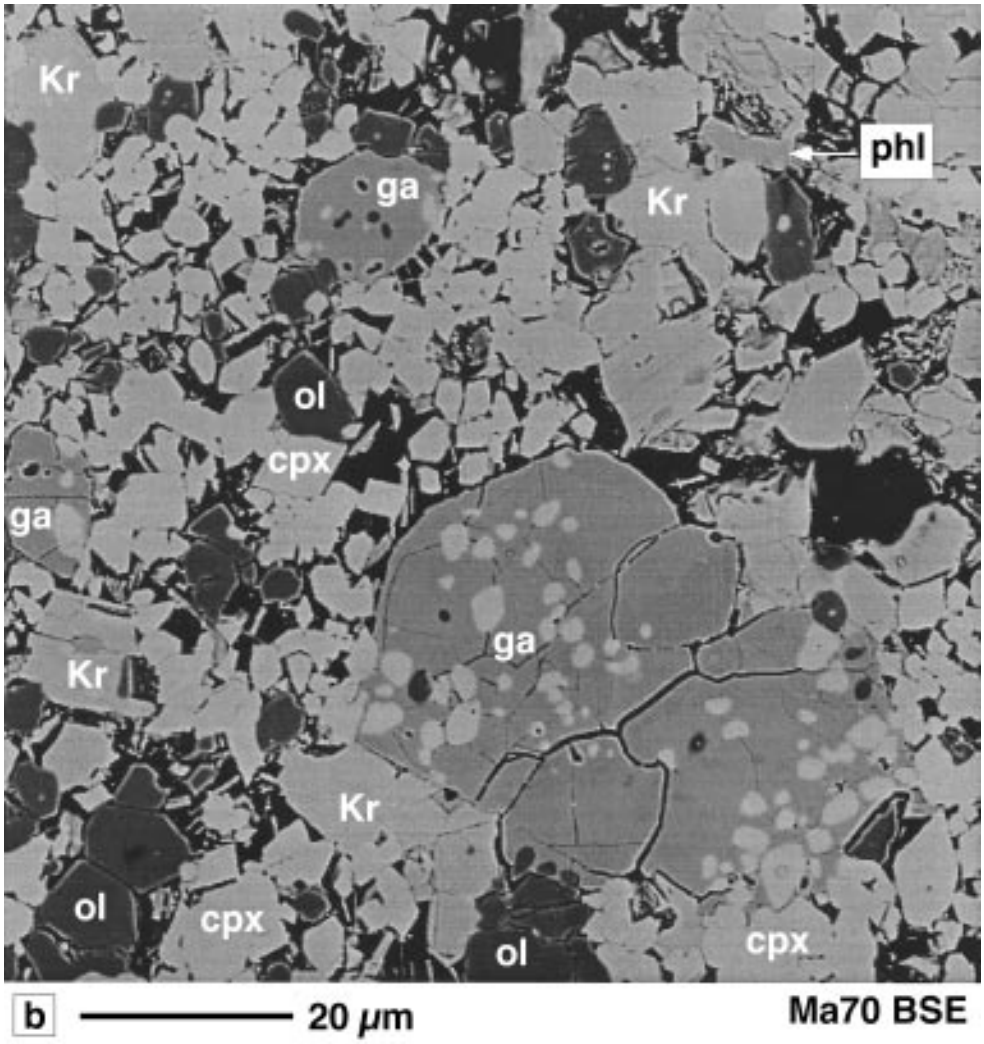

Fig. 3. Backscattered electron photomicrographs (a) of the assemblage K-richterite + phlogopite + clinopyroxene in run Ma42 (Kr-field I) and (b) of the assemblage K-richterite + garnet + phlogopite + clinopyroxene + olivine + quench in run Ma70 (Kr-field II). Run conditions are listed in Table 2.

+ olivine + quench (Fig. 5). Phase relations within these two regions are discussed separately.

Kr-field I. The stable assemblage in Kr-field I is K-richterite + phlogopite + clinopyroxene. At pressures $\geq 7{\cdot}0$ GPa trace amounts of olivine appear, associated with small amounts (<5 vol. %) of coarse-grained, extremely acicular quench-phlogopite. Phlogopite + olivine are considered products of incongruent phlogopite dissolution in a fluid at subsolidus conditions. The quench phlogopites are consistently depleted in Al and enriched in Si compared with texturally stable phlogopites (see Table 4, below).

The lower pressure stability limit of K-richterite at 900°C is between 1·0 and 1·5 GPa; below that pressure, the stable assemblage is phlogopite + clinopyroxene. Using idealized end-member compositions, a possible model reaction which describes the formation of K-richterite is

$$3CaMgSi_2O_6 + 7NaMg_3AlSi_3O_{10}(OH)_2 + 3K_2O_{fluid} + 14SiO_{2fluid} = 3KNaCaMg_5Si_8O_{22}(OH)_2 + 3KMg_3AlSi_3O_{10}(OH)_2 + 4NaAlSi_2O_6 + H_2O. \quad (1)$$

Reaction (1) is consistent with the strong decrease of Na in phlogopite between 1·0 and 1·5 GPa. K_2O and SiO_2 are considered to be dissolved in the vapour phase. An increase of the jadeite component in clinopyroxene predicted by reaction (1), however, cannot be observed. A likely explanation is that the actual and idealized mineral compositions have different K/Na ratios; in particular, the Na component in K-richterite at 1·5 GPa is considerably larger than that in the idealized formula in equation (1).

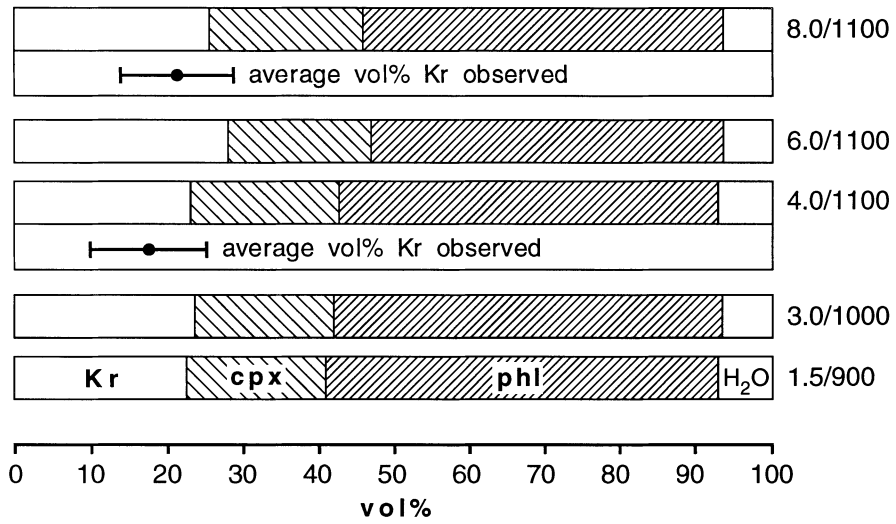

Fig. 4. Calculated and observed modal amounts of mineral phases in selected experimental runs. Numbers refer to pressure (GPa) and temperature (°C) of the experiments. Horizontal bars give the calculated modal amounts of the phases K-richterite (Kr), clinopyroxene (cpx), phlogopite (phl) and water; for comparison, black dots denote the actually observed modal amount of K-richterite averaged by image analysis from nine representative areas within two runs at 8·0 GPa and 1100°C and at 4·0 GPa and 1100°C.

The upper T stability limit of K-richterite in Kr-field I has been determined at 4·0, 6·0 and 7·0 GPa. At 4·0 GPa, K-richterite breakdown occurs between 1135 and 1200°C. This can be concluded from the phase distribution in run Ma34 which contains two distinctly different assemblages adjacent to each of the two separated thermocouples. At the capsule bottom (thermocouple reading 1200°C), phlogopite + clinopyroxene + olivine + extremely coarse-grained quench is encountered. The quench makes up ~20 vol. % of the entire charge. The second thermocouple, attached to the capsule wall close to the capsule tip ~1000 μm from the quench–solid boundary, had a temperature reading of 1136°C, and the assemblage comprised K-richterite + phlogopite + clinopyroxene. The boundary between K-richterite-present and K-richterite-absent assemblages is ~650–750 μm from the quench–solid boundary. At 4·0 GPa and 1250°C the texturally stable assemblage is phlogopite + clinopyroxene + olivine + quench. Between 1200 and 1250°C phlogopite and clinopyroxene show a slight but significant change in chemistry, as will be discussed below. At the same time, the grain size of the quench changes from extremely coarse to almost glassy, which firmly establishes that above-solidus conditions must have been reached between 1200 and 1250°C. Runs Ma75, at 6·0 GPa and 1300°C, and Ma78, at 7·0 GPa and 1300°C, both lack K-richterite and contain <5% quench.

Kr-field II. The Kr-field II is a narrow interval above 7·0 GPa and at 1200°C < T < 1400°C. The assemblage at 8·0 GPa and 1300°C contains garnet with K-richterite + clinopyroxene + phlogopite + olivine + quench. Between 1300 and 1400°C both K-richterite and phlogopite disappear, giving rise to a garnet + clinopyroxene + olivine + quench assemblage. The formation of garnet is due to a continuous phlogopite-breakdown reaction as evidenced by coexisting phlogopite + garnet. The potassium released during the reaction is accommodated on the M(4)-site of amphibole as KKCa-richterite component, as will be discussed in the next section. In Kr-field II the K/OH ratio of K-richterite is much higher than that of phlogopite. Amphibole (and garnet) formation from phlogopite therefore produces excess H_2O, which may trigger K-richterite breakdown and melting with a further increase in temperature. Expressed in terms of idealized end-members, the reaction that produces KKCa-richterite component is

$$12KMg_3AlSi_3O_{10}(OH)_2 + 21CaMgSi_2O_6 = 6KKCaMg_5Si_8O_{22}(OH)_2 + 5Ca_3Al_2Si_3O_{12} + Mg_3Al_2Si_3O_{12} + 12Mg_2SiO_4 + 6H_2O \quad (2)$$

or, in a more general form

$$\text{phlogopite} + \text{clinopyroxene}_{ss} \rightarrow \text{KK-richterite}_{ss} + \text{garnet}_{ss} + \text{olivine} + H_2O. \quad (2a)$$

The above reaction is equivalent to the K-amphibole-forming reaction in the system KCMASH

$$4KMg_3AlSi_3O_{10}(OH)_2 + 2CaMgSi_2O_6 = KKCaMg_5Si_8O_{22}(OH)_2 + 2Ca_{0.5}Mg_{2.5}Al_2Si_3O_{12} + 2Mg_2SiO_4 + K_2O + 6H_2O \quad (3)$$

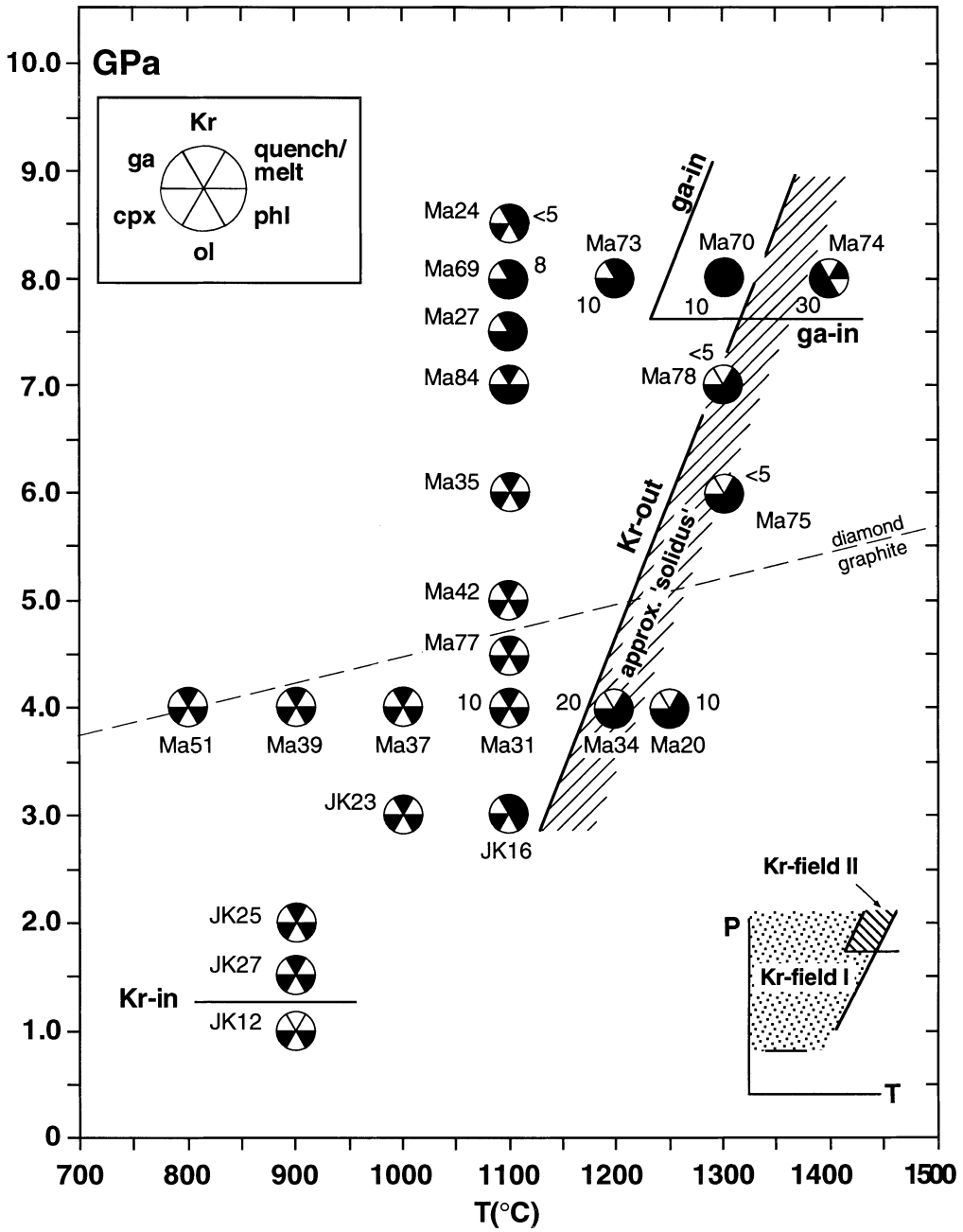

Fig. 5. *P–T* diagram summarizing experimental results in the KNCMASH system using experimental bulk composition 1 (see Table 1). Phases present in the experimental charge are represented by black sectors within the run symbol, phases not detected are denoted by white sectors (inset upper left). The dashed line is the graphite–diamond boundary as given by Kennedy & Kennedy (1976). Insert sketch at bottom right represents *P–T* stability fields of K-richterite without garnet (Kr-field I) and K-richterite plus garnet (Kr-field II) (see text). Numbers next to run symbols give the vol. % of quench observed in the charge. Piston-cylinder runs are labelled with JK, multi-anvil runs with Ma (see Table 2).

proposed by Sudo & Tatsumi (1990), and provides a link between the KNCMASH and KCMASH systems.

Whereas the amount of quench between 1100 and 1300°C remains nearly constant at ~10 vol. %, there is an increase to 30% at 1400°C. This is taken as an indication for crossing the solidus between 1300 and 1400°C. Thus, we consider that the quench observed in smaller volumes at lower temperatures is more probably

from a subsolidus fluid than from a melt. This conclusion is also true for experiments at 4·0 GPa.

In view of the strong solubility of K_2O and SiO_2 in high-P aqueous fluids, the question whether selective removal of the potassium component can shift the solid-bulk from peralkaline to subalkaline [the term subalkaline will be used to refer to bulk compositions with molar $(K_2O + Na_2O)/Al_2O_3 < 1$] must be considered. Experiments on subalkaline peridotite-like bulk compositions (above the omphacite–olivine tie-line in Fig. 1) have produced K-richterite coexisting with garnet (Sudo & Tatsumi, 1990). Ryabchikov & Boettcher (1980) and Schneider & Eggler (1986) showed that substantial phlogopite can be dissolved in aqueous vapour between 1·0 and 3·0 GPa. If the solution mechanism is incongruent dissolution of phlogopite to olivine + vapour (Modreski & Boettcher, 1972) then the vapour must contain considerable dissolved Al_2O_3 as well as K_2O, MgO and SiO_2. In the course of this study, a reconnaissance run with $K_2O/H_2O = 0{\cdot}10$ was conducted at 8·0 GPa and 1100°C. This run failed to stabilize any solid K-phase but produced extensive amounts of low Al-quench-phlogopite. This provides evidence for substantial Mg and some Al dissolved in the aqueous fluid at high P and T.

Leaching of phlogopite, congruent or incongruent, will not change the solid bulk from peralkaline to subalkaline, as the bulk would move in a direction approximately perpendicular or parallel to the olivine–omphacite tie-line shown in Fig. 1. It is only by selective removal of K_2O that the solid bulk composition would eventually reach subalkaline chemistry. From the solution studies mentioned above, however, there is no evidence for such a mechanism. Although quench phlogopite contains some Na ($\leq 0{\cdot}5$ wt % Na_2O), dissolution of clinopyroxene was considered negligible compared with that of phlogopite. These considerations suggest that stability of K-richterite + garnet is an intrinsic feature of peralkaline systems at high P and T.

Comparison of KNCMASH results with phase relations of natural MARID AJE137 at P >4·0 GPa

To compare the phase relations of natural MARID AJE137 with those of the synthetic system at P >4·0 GPa, six additional experiments were conducted using AJE137 as a starting material (Table 2). The results, given in Fig. 6, are consistent with phase relations determined by Sweeney *et al.* (1993) to 3·0 GPa as well as with results in the synthetic system. The K-richterite-out curve is only shifted by 50–100°C toward lower temperatures in the natural composition compared with the KNCMASH system described above. Most importantly, garnet appears subsolidus in the natural bulk system AJE137 at 7·5 GPa and 1180°C coexisting with orthopyroxene + clinopyroxene + K-richterite + phlogopite. This is consistent with its appearance at slightly higher temperatures (>1250°C) at similar pressures in KNCMASH (Fig. 5). In bulk composition AJE137, garnet was also found in three above-solidus runs at 4·6, 6·8 and 7·5 GPa coexisting with clinopyroxene + orthopyroxene + olivine + melt (Fig. 6).

Comparison with previous results

The position of the K-richterite-out reaction in the KNCMASH system is in good agreement with results of Sweeney *et al.* (1993). The solidus at 4·0 GPa in the KNCMASH system, however, is depressed by ~50–100°C compared with the results (Fig. 7) of Sweeney *et al.* (1993) and Van der Laan & Foley (1994), with no evidence for an extended subsolidus K-richterite-absent region. There are two possible explanations for this discrepancy:

(1) The observed 'solidus' in the natural system AJE137 is the true solidus. The subsolidus K-richterite-absent region in the natural system would therefore be due to amphibole dehydration, resulting in a K-richterite-free H_2O-saturated subsolidus assemblage.

(2) There is an extended P–T range in the natural system where very small and optically undetectable amounts of melt are present. In this case K-richterite-out and the real solidus coincide. Mass balance calculations by Sweeney *et al.* (1993) suggest that incongruent melting of K-richterite must produce >5 vol. % melt. The 'solidus' given by Sweeney *et al.* (1993) can be interpreted as the P–T condition where incongruent melting of phlogopite and K-richterite begins and produces easily observed amounts of melt. Whereas garnet appeared above-solidus in AJE137 runs at P>4·6 GPa, MARID melt experiments by Van der Laan & Foley (1994) did not yield garnet up to 1500°C at 5·0 GPa. A possible explanation for the absence of garnet is Fe loss to the capsule, which would destabilize garnet.

Enstatite is absent from the KNCMASH system over the entire P–T range investigated. Instead, olivine appears above the solidus and also coexists with K-richterite at high pressures. Clinopyroxene + olivine + melt at 1250°C and 4·0 GPa can be explained in terms of incongruent melting of K-richterite (Gilbert & Briggs, 1974) and/or phlogopite (Yoder & Kushiro, 1969). Clinopyroxene + olivine + melt was also observed by Van der Laan & Foley (1994) using a rutile-free mixture of natural K-richterite + phlogopite + clinopyroxene. Addition of rutile to the starting material resulted in the appearance of enstatite at 5·0 GPa, but not in runs at 1·5 GPa. This is consistent with results of Sweeney *et al.* (1993), who observed a transition from olivine to enstatite

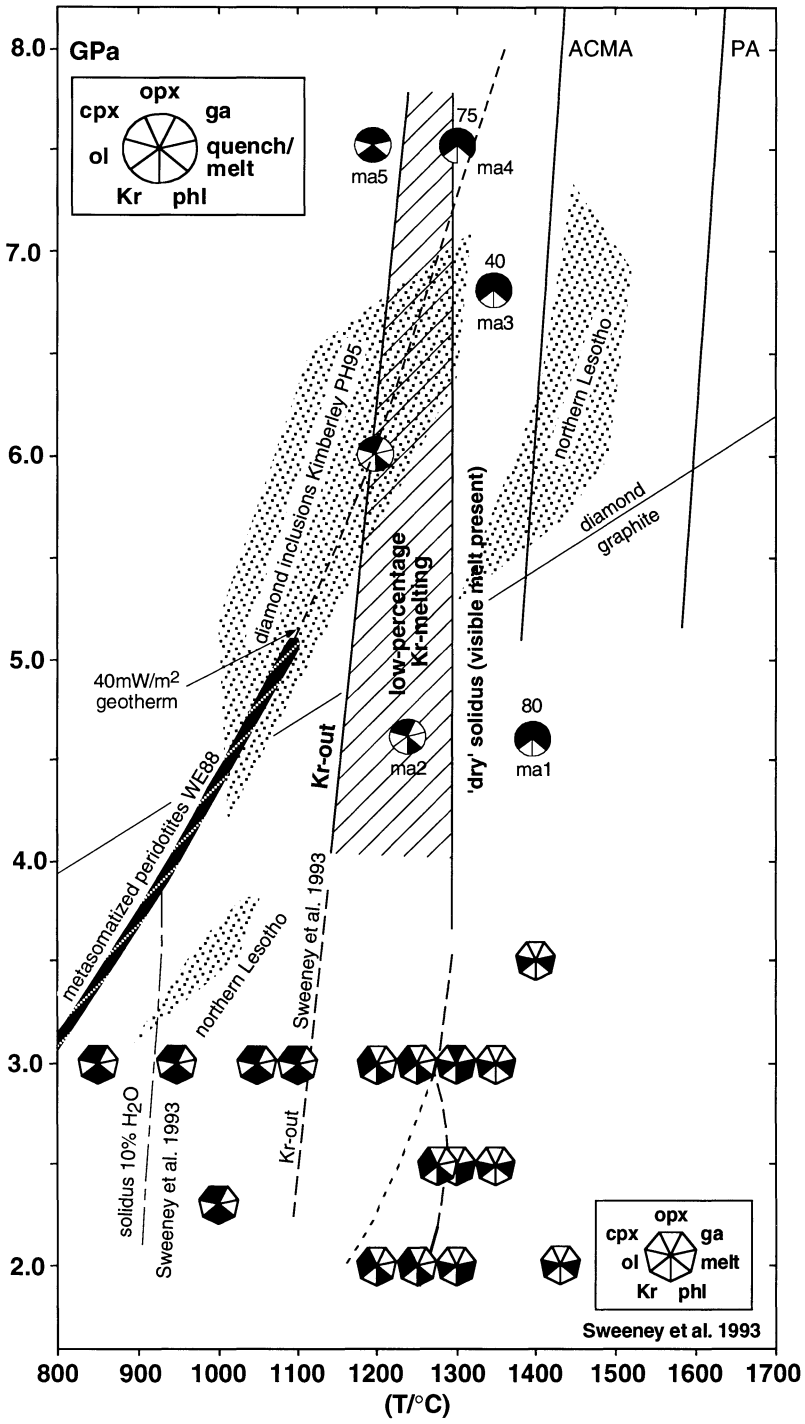

Fig. 6. *P–T* diagram summarizing experimental results for natural MARID AJE137. Circles are run symbols for experiments of the present study, heptagons denote experiments by Sweeney *et al.* (1993). Meaning of symbols as in Fig. 5 (inset upper left); numbers next to run symbols are approximate percentages of melt in the charge. The dashed line is a 40 mW/m^2 geotherm according to Pollack & Chapman (1977); diamond–graphite equilibrium as in Fig. 5. ACMA and PA are the average current mantle adiabat for a surface potential temperature of 1280°C and a plume adiabat as given by Thompson (1992); shaded areas span the *P–T* range obtained from clinopyroxene–orthopyroxene–garnet geothermobarometry; WE88—Waters & Erlank (1988), *P–T* for metasomatized peridotites; PH95—Phillips & Harris (1995), *P–T* for diamond inclusions from the Kimberley area; northern Lesotho: *P–T* derived from garnet peridotite data given by Nixon & Boyd (1973) (table 20a) using the experimental calibrations of Brey & Köhler (1990) for the garnet–orthopyroxene barometer and for the clinopyroxene–orthopyroxene solvus thermometer.

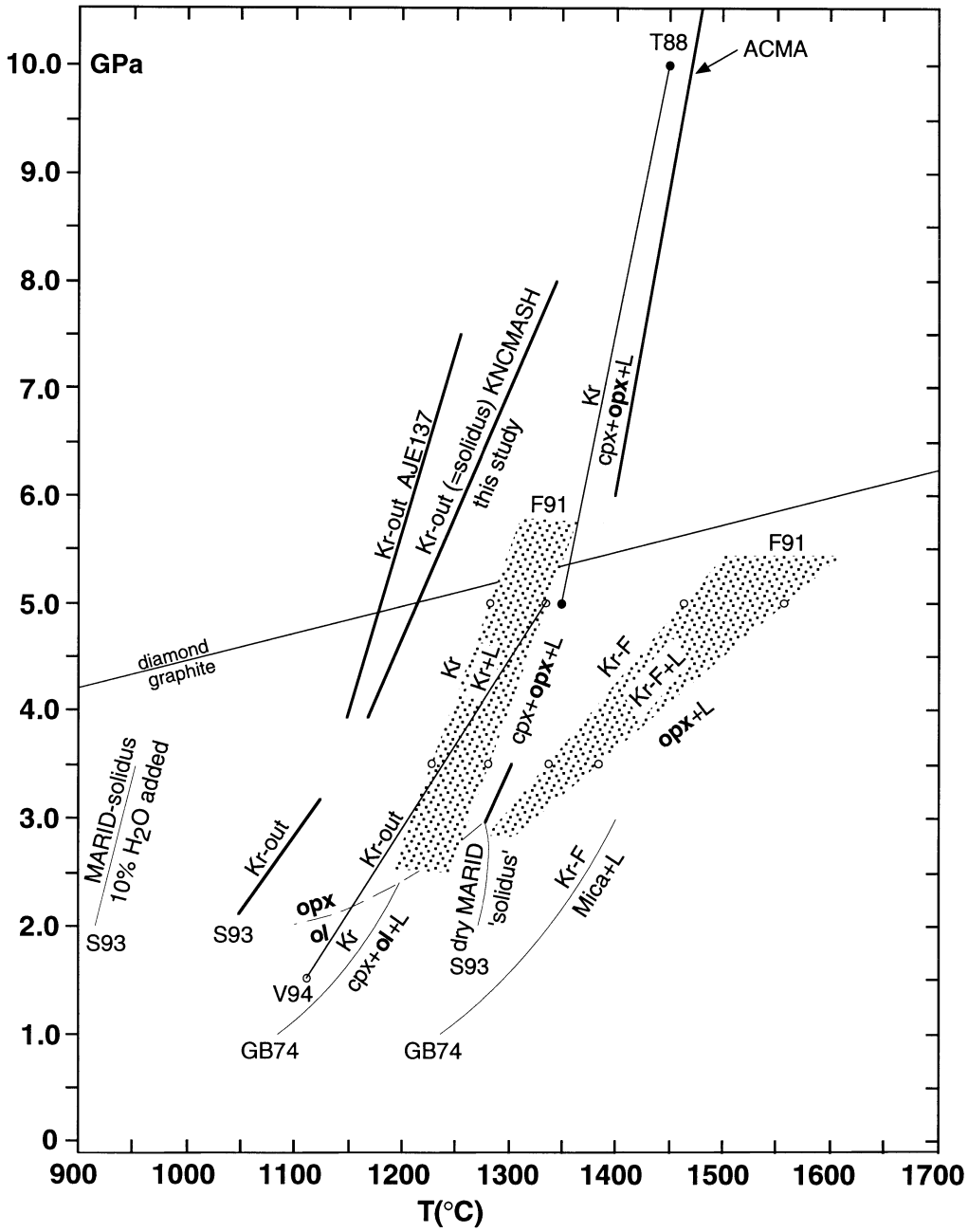

Fig. 7. *P–T* diagram summarizing experimental results on K-richterite stability in various bulk compositions: S93—Sweeney *et al.* (1993), natural MARID AJE137; GB74—Gilbert & Briggs (1974), F91—Foley (1991), pure synthetic K-richterite and K-F-richterite; V94—Van der Laan & Foley (1994), equal weight proportions of natural K-richterite, phlogopite and clinopyroxene; T88—Trønnes *et al.* (1988), pure synthetic K-richterite. Graphite–diamond equilibrium as in Fig. 5 and the ACMA as in Fig. 6.

with increasing pressure [modal analysis of AJE137 contains 1·2% rutile; see Waters (1987*b*)]. It is concluded that in peralkaline MARID-like bulk compositions, Ti acts as a network-former, which in addition to high pressure, promotes polymerization of the melts formed by K-richterite breakdown. This is necessary to stabilize orthopyroxene, whose structure is more polymerized than that of olivine. For pure K-richterite, because of its much higher Si content (57·6 wt % SiO_2 compared with 47·6% in bulk I), the transition from olivine (Gilbert & Briggs,

1974) to enstatite (Foley, 1991) as a K-richterite breakdown product is a function of pressure. The P range of this transition is similar to that observed in the natural MARID-bulk investigated by Sweeney *et al.* (1993) (see Fig. 7).

Mineral chemistry

Amphibole

According to the nomenclature of Leake (1978) modified by Hawthorne (1983), all amphiboles synthesized in this study are true K-richterites. This end-member can be represented as a combination of

$$\square Ca_2Mg_5Si_8O_{22}(OH)_2 + NaSiCa_{-1}Al_{-1}\ (pl) + NaAl\square_{-1}Si_{-1}\ (ed) + KNa_{-1}\ (kn) = KNaCaMg_5Si_8O_{22}(OH)_2 \quad (4)$$

where the three vectors pl, ed and kn are obtained using the method of Thompson *et al.* (1982). The scheme outlined above is based on the assumption that potassium, because of its large ionic radius, does not enter the M(4)-site. Sudo & Tatsumi (1990), however, were able to synthesize pure K-amphiboles with the formula $KKCaMg_5Si_8O_{22}(OH)_2$ in the KCMASH system. Also in the present study in KNCMASH, amphiboles with K >1·0 p.f.u. (per formula unit) were stabilized. Apart from experimental evidence, K-richterites from MARID xenoliths recovered from the Newlands group II kimberlite are known to contain >1·0 K p.f.u. [see BD1778 in table 3 of Dawson & Smith (1977)]. To account for K(M4), pl, ed and kn vectors can be combined such that

$$\square Ca_2Mg_5Si_8O_{22}(OH)_2 + NaSiCa_{-1}Al_{-1} + NaAl\square_{-1}Si_{-1} + 2KNa_{-1} = KKCaMg_5Si_8O_{22}(OH)_2$$

which affects both A- and M(4)-sites. (5)

Kr-field 1. The most pronounced variation in amphibole chemistry occurs in the K and Na content. K increases from 0·75 p.f.u. at 1·5 GPa and 900°C to 1·03 at 8·5 GPa and 1100°C. At the same time, Na decreases from 1·03 to 0·84 p.f.u. (Fig. 8). This results in an increase of X_K, i.e. K(A)/[K(A) + Na(A) + Na(M4)], in K-richterite, with K only on the A-site, from 0·42 to 0·55 (Fig. 8). This change in X_K is mainly due to increasing KNa_{-1} on the A-site with K/[K + Na(A)] changing from 0·78 at 1·5 GPa and 900°C to 1·00 (A-site fully occupied by K) at 8·5 GPa and 1100°C. A minor change of Na(M4) of only ~0·08 p.f.u. (Fig. 8) does not contribute significantly to the overall increase of X_K. Ca(M4) in the amphiboles is directly connected to the behaviour of Na(M4) because only very small amounts of Mg(M4) are present as a cummingtonite component (0·01–0·05 p.f.u.). No systematic variation of Mg(M4) with either pressure or temperature could be observed. Within Kr-field I, runs at 8·0 and 8·5 GPa contain amphiboles with K slightly greater than 1·0 p.f.u. Site assignment yields constant K(M4) for Ma73 with an average of 0·04 ± 0·022 (n = 10).

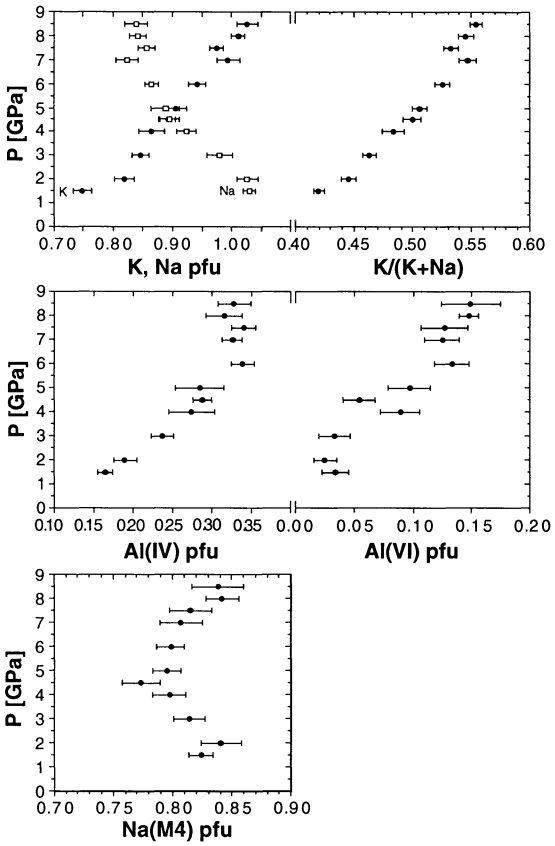

Fig. 8. Selected mineral chemical parameters of K-richterite as a function of P (and T). The temperature for runs from 4·0 to 8·5 GPa is 1100°C; below 4·0 GPa, run conditions are 1·5 GPa and 900°C, 2·0 GPa and 900°C, and 3·0 GPa and 1000°C. Individual data points represent averaged values of 4–12 analyses (see Table 3).

All analysed amphiboles show an A-site occupancy very close to 1·0 with a maximum average vacancy of 0·05 p.f.u. at 1·5 GPa and 900°C. (K + Na) on the A-site is very sensitive to analytical errors: cation-numbers >16·00, though theoretically impossible, may arise from statistical errors of microprobe analyses; they are transformed to (K + Na)(A) >1·0 during the site assignment.

Aluminium is a minor constituent of all analysed amphiboles, with a maximum value of 0·44 p.f.u. found for K-richterites in Kr-field I at 8·5 GPa and 1100°C. Al is present both as Al(VI) and Al(IV) (Fig. 8). Octahedral Al is introduced by the Tschermaks-exchange (tk) Al(IV)Al(VI)$Mg_{-1}Si_{-1}$; it increases with pressure at constant temperature (isothermal part of Fig. 8 from 4·0 to 8·5 GPa) to a maximum value of 0·15 p.f.u. In ideal pure

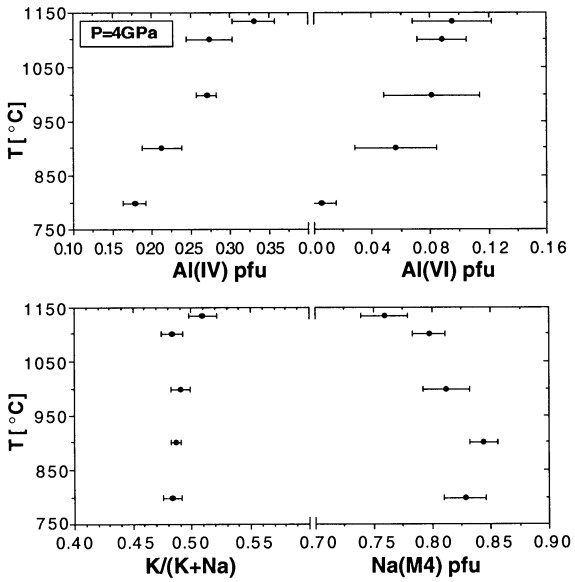

Fig. 9. Selected mineral chemical parameters of K-richterite in an isobaric section at 4·0 GPa from 800°C to the temperature of the K-richterite-out reaction (1100°C<T<1150°C). Individual data points represent averaged values of 6–14 analyses (see Table 3).

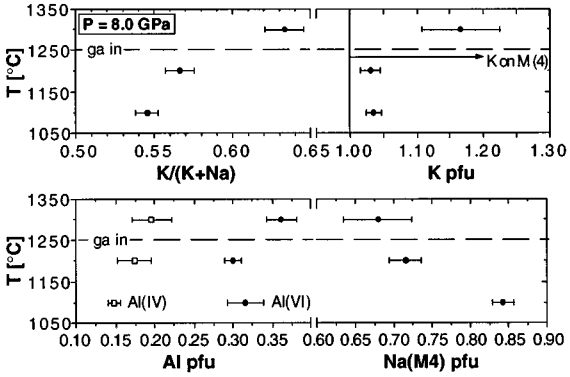

Fig. 10. Selected mineral chemical parameters of K-richterite in an isobaric section at 8·0 GPa from 1100°C to the temperature of the K-richterite-out reaction (1300°C<T<1400°C). The dashed horizontal line denotes temperature of the appearance of garnet (Kr-field I–Kr-field II boundary). Individual data points represent averaged values of 6–11 analyses (see Table 3).

K-richterite no tetrahedral Al occurs, because it is balanced by the combined operation of ed and pl vectors [see equation (4)]. In the present experiments, however, ed vector>pl vector, resulting in tetrahedral Al with an amount increasing to 0·33 p.f.u. at 8·5 GPa and 1100°C.

To separate temperature effects on amphibole chemistry from pressure effects, an isobaric series of experiments at 4·0 GPa was conducted from 800 to 1200°C. The results are summarized in Fig. 9. The most significant changes are an increase in tk component accompanied by a slight decrease in pl component, the latter showing no significant influence on X_K, which remains essentially constant over the whole T interval investigated.

Kr-field II. Amphiboles in run Ma70 (8·0 GPa and 1300°C) coexisting with garnet are characterized by a drastic increase in K compared with run Ma73. The average value for K(M4) is 0·154 ± 0·021 (n = 11), $X_{K,amph}$ and $Al_{tot,amph}$ increase to 0·63 and 0·57 p.f.u., respectively, which represent the maximum values for K-richterites found in this study. K-richterite coexisting with garnet in natural MARID AJE137 is characterized by a similar high K content. Two analyses yield K(M4) of 0·257 and 0·258 p.f.u., respectively (see Table 7, below). Figure 10 shows the change in amphibole chemistry in an isobaric section at 8·0 GPa across the Kr-field I–Kr-field II boundary for the KNCMASH system. Averaged analyses of K-richterites are listed in Table 3.

Phlogopite

Measured phlogopites are close to ideal end-member composition. Variation occurs in the Na and Al contents. The most pronounced change in chemistry can be observed with the first appearance of K-richterite between 1·0 and 1·5 GPa. Na and Al_{tot} in phlogopite both decrease from 0·07 and 1·12 p.f.u. in the assemblage phlogopite + clinopyroxene to 0·02 and 0·98 p.f.u. in Kr-field I (Fig. 11a). Once K-richterite is stable there is little further variation in phlogopite chemistry with increasing pressure: only K/(K + Na) exhibits a slight increase at constant temperature, which is, however, much less pronounced than that in coexisting K-richterite (Fig. 12). The inverse correlation of Na content and pressure is also present in natural AJE137 runs. Al(VI) is present in all phlogopites in small amounts up to 0·04 p.f.u. Values of Al(IV) <1·0 can be attributed to an edenite exchange towards talc, which is equivalent to phlogopite – [Na(A)Al(IV)$\square_{-1}$Si$_{-1}$ + KNa$_{-1}$]. This exchange also creates a vacancy on the interlayer site. Most analysed phlogopites have a small vacancy on the octahedral site of up to 0·02 p.f.u. owing to an $\square$ Al_2Mg_{-3} exchange towards dioctahedral structure. Alternatively, Al(IV) <1·0 and the vacancy on the octahedral site may be explained by an exchange $\square Si_2Mg_{-1}Al(IV)_{-2}$ towards montdorite, $K(Mg_{2.5}\square_{0.5})[Si_4O_{10}](OH)_2$, a tetrasilicic mica (Seifert & Schreyer, 1971). Experimental work of Harlow (1995) showed montdorite to be stable to 8–11 GPa at 1350–1450°C in synthetic mixtures of diopside + talc + KCl.

In the 4·0 GPa isobaric section no major changes in chemistry occur between 800 and 1200°C. At 1250°C a sudden increase in Al_{tot} from a constant value of ~1·0 to ~1·06 can be observed. This was taken as an indication

Table 3: Average analyses of K-richterites from high-pressure experiments

Experiment:	JK27	JK25	JK23	JK22	Ma31	Ma71	Ma72	Ma79	Ma77	Ma42	Ma35	Ma84	Ma27	Ma69	Ma73	Ma70	Ma24	Ma37	Ma39	Ma51
Bulk comp.:	1	1	1	4	1	2	3	4	1	1	1	1	1	1	1	1	1	1	1	1
P (GPa):	1·5	2·0	3·0	3·0	4·0	4·0	4·0	4·0	4·5	5·0	6·0	7·0	7·5	8·0	8·0	8·0	8·5	4·0	4·0	4·0
T (°C):	900	900	1000	1000	1100	1100	1100	1100	1100	1100	1100	1100	1100	1100	1200	1300	1100	1000	900	800
No. of analyses:	8	9	12	4	10	6	7	4	11	9	10	10	12	6	10	11	9	8	14	7
SiO_2	57·23(25)	56·86(13)	56·74(22)	57·33(12)	56·21(33)	55·84(19)	55·41(09)	55·95(31)	55·86(23)	56·53(53)	55·25(35)	55·43(29)	55·38(47)	55·96(37)	55·73(42)	55·56(27)	55·47(40)	56·44(16)	56·91(45)	56·71(27)
Al_2O_3	1·23(07)	1·34(08)	1·67(08)	0·93(06)	2·24(13)	2·78(13)	3·70(25)	1·17(02)	2·11(06)	2·37(22)	2·69(35)	2·76(09)	2·87(12)	2·86(17)	3·13(08)	3·52(08)	2·93(13)	2·25(21)	1·66(24)	1·14(14)
MgO	24·47(22)	24·44(14)	24·39(17)	24·46(07)	23·98(15)	24·34(17)	24·20(17)	24·03(15)	24·12(22)	24·12(22)	24·00(20)	23·77(18)	23·81(36)	23·78(14)	23·74(15)	23·88(23)	23·68(18)	24·16(17)	24·31(17)	24·39(19)
CaO	7·84(10)	7·85(13)	8·04(12)	7·88(06)	8·11(08)	8·14(09)	8·25(10)	7·99(11)	8·17(09)	8·18(08)	7·93(13)	7·83(13)	7·77(10)	7·68(09)	7·65(14)	7·42(11)	7·53(15)	7·91(10)	7·80(09)	7·75(14)
Na_2O	3·89(03)	3·86(06)	3·69(09)	2·69(08)	3·48(06)	3·69(06)	4·09(10)	2·35(09)	3·34(06)	3·35(10)	3·23(05)	3·07(07)	3·20(04)	3·16(06)	2·96(10)	2·53(09)	3·13(07)	3·47(05)	3·58(05)	3·57(09)
K_2O	4·28(10)	4·68(10)	4·85(07)	6·45(06)	4·93(12)	4·26(02)	3·61(08)	6·56(10)	5·06(09)	5·20(08)	5·35(11)	5·63(10)	5·52(09)	5·84(09)	5·87(08)	6·63(15)	5·90(07)	5·10(11)	5·14(08)	5·05(07)
H_2O	2·19(01)	2·19(01)	2·19(01)	2·19(01)	2·18(01)	2·19(01)	2·20(00)	2·15(01)	2·17(01)	2·20(02)	2·17(01)	2·17(01)	2·17(02)	2·19(01)	2·18(01)	2·19(01)	2·17(01)	2·19(01)	2·18(03)	2·17(01)
Σ	101·12(45)	101·22(19)	101·57(53)	101·93(32)	101·13(34)	101·23(39)	101·46(26)	100·21(56)	100·83(51)	101·94(67)	100·61(39)	100·65(35)	100·72(83)	101·47(42)	101·26(62)	101·73(42)	100·80(47)	101·52(26)	101·38(48)	100·79(41)
Si	7·835(09)	7·800(14)	7·764(18)	7·853(11)	7·726(28)	7·650(16)	7·561(25)	7·808(01)	7·711(11)	7·715(31)	7·643(22)	7·674(13)	7·660(16)	7·685(23)	7·666(18)	7·627(13)	7·672(21)	7·730(13)	7·787(26)	7·818(15)
Al	0·199(12)	0·217(12)	0·269(12)	0·150(10)	0·368(11)	0·449(21)	0·596(39)	0·173(38)	0·343(10)	0·384(34)	0·452(42)	0·451(16)	0·467(21)	0·463(29)	0·508(10)	0·569(15)	0·477(22)	0·359(31)	0·268(38)	0·186(22)
Mg	4·992(27)	4·997(27)	4·974(17)	4·993(04)	4·918(32)	4·970(20)	4·922(33)	4·993(12)	4·963(29)	4·899(28)	4·953(35)	4·905(24)	4·9091(37)	4·868(11)	4·869(32)	4·886(35)	4·883(40)	4·940(33)	4·958(35)	5·012(35)
Ca	1·150(18)	1·154(18)	1·179(14)	1·156(07)	1·195(11)	1·194(13)	1·207(14)	1·195(11)	1·209(10)	1·196(14)	1·179(14)	1·162(21)	1·152(16)	1·130(16)	1·128(23)	1·091(14)	1·116(23)	1·160(17)	1·143(16)	1·144(21)
Na	1·031(10)	1·027(17)	0·980(22)	0·714(22)	0·925(17)	0·979(18)	1·082(26)	0·637(29)	0·894(18)	0·888(28)	0·865(11)	0·823(19)	0·858(14)	0·842(14)	0·791(23)	0·673(35)	0·839(19)	0·928(20)	0·948(15)	0·955(23)
K	0·748(16)	0·819(17)	0·846(14)	1·127(08)	0·865(22)	0·744(06)	0·629(13)	1·189(44)	0·892(13)	0·905(18)	0·942(15)	0·994(19)	0·974(12)	1·024(14)	1·030(16)	1·161(26)	1·041(11)	0·891(20)	0·898(16)	0·889(14)
Σ	15·955(16)	16·015(11)	16·017(16)	15·992(16)	15·990(28)	15·986(12)	15·996(11)	15·996(15)	16·010(09)	15·989(34)	16·032(16)	16·012(13)	16·019(15)	16·012(08)	16·003(06)	16·012(15)	16·028(19)	16·003(07)	16·002(31)	16·013(09)
K/(K+Na)	0·420(05)	0·443(05)	0·463(06)	0·612(08)	0·483(09)	0·432(03)	0·368(09)	0·647(11)	0·499(08)	0·506(06)	0·521(05)	0·547(07)	0·532(06)	0·549(04)	0·566(09)	0·633(12)	0·554(05)	0·492(07)	0·486(04)	0·482(08)

Amphibole formulae recalculated to 23 oxygens + stoichiometric OH. Numbers in parentheses denote 1σ standard deviation (57·23 ± 0·25; 7·835 ± 0·009).

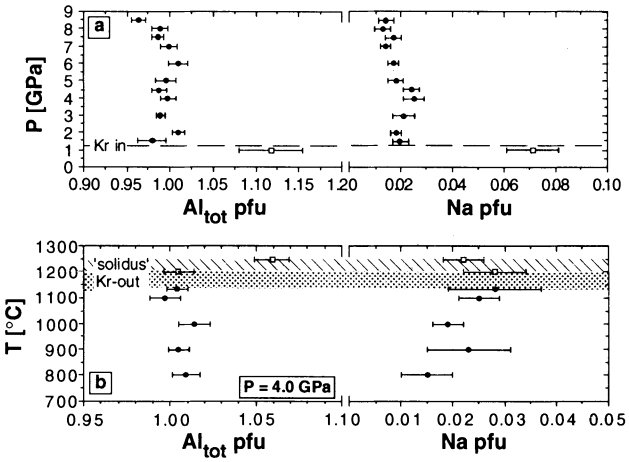

Fig. 11. (a) Selected mineral chemical parameters of phlogopite as a function of *P* (and *T*). *P–T* conditions for runs as in Fig. 8 except for additional run at 1·0 GPa and 900°C below the K-richterite-in reaction. The dashed horizontal line denotes pressure of the appearance of K-richterite. Individual data points represent averaged values of 6–11 analyses (see Table 4). (b) Selected mineral chemical parameters of phlogopite in an isobaric section at 4·0 GPa from 800°C to the temperature of the supposed 'solidus' (1200°C<*T*<1250°C). Hatched horizontal bars denote approximate location in temperature of the K-richterite-out reaction and the 'solidus' as derived from textural and mineral chemical criteria (see text). Individual data points represent averaged values of 8–12 analyses (see Table 4).

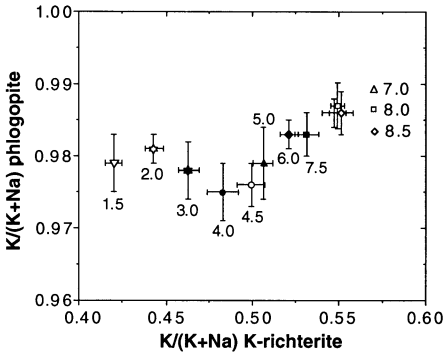

Fig. 12. Variation of K/(K + Na) in K-richterite and coexisting phlogopite as a function of *P* (and *T*). Numbers give the pressure conditions of individual runs with run temperatures as in Fig. 8. Each point represents an average of 4–12 K-richterite and 6–11 phlogopite analyses (see Tables 3 and 4).

for crossing the solidus (Fig. 11b). This contention is supported by textural evidence as well as by a concomitant change in clinopyroxene chemistry (see below). Averaged analyses of phlogopite are listed in Table 4.

Clinopyroxene

Clinopyroxenes in this study can be described as diopside–jadeite–enstatite solid solutions. Na and Al_{tot} show a 1:1 correlation which excludes any significant Ca-Tschermaks component. Small amounts of Ca-Tschermaks component in the analysed clinopyroxenes ($\leq$0·015 p.f.u.) may be artefacts which arise from deficits in Si analyses owing to analytical errors.

Within the Kr-field I, clinopyroxenes are essentially binary jadeite–diopside solid solutions with maximum enstatite contents of ~6 mol %. The jadeite component continuously increases with increasing pressure from $jd_4di_{92}en_2$ at 1·5 GPa and 900°C to $jd_{20}di_{75}en_5$ at 8·5 GPa and 1100°C. The appearance of amphibole between 1·0 and 1·5 GPa does not influence clinopyroxene chemistry. With increasing jadeite content Ca/Mg continuously decreases, owing to the slight increase in Mg(M2).

At 8·0 GPa the enstatite component becomes important with increasing temperature: it changes across the Kr-field I–Kr-field II boundary from $jd_{17}di_{77}en_6$ at 8·0 GPa and 1200°C to $jd_{19}di_{69}en_{12}$ and further to $jd_{17}di_{63}en_{19}$ above the solidus at 8·0 GPa and 1400°C. At the same time, Ca decreases from 0·80 to 0·65 p.f.u.

Measured K_2O contents of clinopyroxene in the present study do not exceed 0·45 wt %. There is a considerable scatter of K values in individual runs, which may, at least in part, be due to beam overlap with adjacent phlogopite and/or K-richterite. On the average, however, there is an increase of K_2O in clinopyroxene with increasing pressure (sample JK12: K_2O = 0·13 $\pm$ 0·06 wt %, n = 12; sample Ma24: K_2O = 0·30 $\pm$ 0·07 wt %, n = 6; compare Table 5). There is no significant difference in K of clinopyroxenes between K-richterite-bearing and K-richterite-absent runs at high *P* (compare runs Ma69 and Ma74). This clearly shows that preferential partitioning of K into the large A-site of coexisting amphibole cannot explain the overall low K contents of clinopyroxenes in high-*P* runs. As these K contents are much lower than in some natural clinopyroxenes, it must therefore be assumed that high K/Na bulk ratios and the presence of trivalent cations other than Al are important for the formation of natural high-K clinopyroxenes (Harlow & Veblen, 1991; Harlow, 1994) in addition to high pressure (Edgar & Vukadinovic, 1993).

In the 4·0 GPa isobaric section a decrease in Na from a constant value of 0·08 to 0·05 p.f.u. at 1250°C indicates the crossing of the solidus. The decrease in Na of clinopyroxene at the transition from subsolidus to above-solidus conditions also occurs in the natural MARID system (see Table 7, below). Averaged analyses of clinopyroxenes are listed in Table 5.

Garnet

Garnets of the present study are pyrope–grossular solid solutions but with only a minor grossular component. X_{Ca} decreases slightly from 0·14 at 1300°C to 0·10 at 1400°C. All analyses have Si >3·0, which would indicate solid solution with pyroxene (majorite component)

Table 4: Average analyses of phlogopites from high-pressure experiments

Experiment:	JK12	JK27	JK25	JK23	Ma31	Ma34	Ma20	Ma71
Bulk comp.:	1	1	1	1	1	1	1	2
P (GPa):	1·0	1·5	2·0	3·0	4·0	4·0	4·0	4·0
T (°C):	900	900	900	1000	1100	1200	1250	1100
No. of analyses:	10	8	9	10	12	7	7	6
SiO_2	42·41(39)	44·05(29)	43·44(38)	44·36(39)	44·04(37)	43·75(20)	43·47(22)	43·98(22)
Al_2O_3	13·67(46)	12·63(20)	12·39(11)	12·28(13)	12·29(13)	12·35(08)	13·06(12)	12·19(09)
MgO	28·49(19)	28·79(24)	29·21(23)	29·10(21)	28·76(17)	28·66(15)	28·67(26)	29·04(25)
CaO	<0·05	0·05(02)	0·05(03)	0·05(04)	<0·05	<0·05	<0·05	<0·05
Na_2O	0·45(15)	0·15(03)	0·14(02)	0·15(01)	0·19(03)	0·21(04)	0·17(03)	0·27(02)
K_2O	10·30(12)	10·28(15)	10·70(08)	10·71(10)	10·85(16)	10·80(13)	10·74(07)	10·42(10)
H_2O	4·32(03)	4·36(02)	4·34(03)	4·39(03)	4·36(03)	4·34(01)	4·36(02)	4·35(01)
Σ	99·68(62)	100·30(54)	100·26(59)	101·03(67)	100·51(50)	100·14(33)	100·52(40)	100·27(32)
Si	2·932(41)	3·027(10)	3·000(08)	3·033(09)	3·032(11)	3·023(06)	2·992(09)	3·028(13)
Al	1·123(39)	0·979(04)	1·010(07)	0·989(05)	0·997(09)	1·005(09)	1·008(09)	0·990(05)
Mg	2·944(21)	2·949(18)	3·004(15)	2·965(16)	2·951(09)	2·952(12)	2·941(19)	2·981(20)
Ca	—	0·003(02)	0·003(02)	0·003(03)	—	—	—	—
Na	0·072(11)	0·020(03)	0·018(02)	0·021(04)	0·025(04)	0·028(06)	0·023(04)	0·036(03)
K	0·911(11)	0·901(12)	0·943(12)	0·934(12)	0·953(17)	0·952(12)	0·943(09)	0·915(11)
Σ	7·980(10)	7·919(13)	7·974(12)	7·943(15)	7·957(17)	7·961(09)	7·958(10)	7·949(13)
K/(K+Na)	0·927(10)	0·979(04)	0·981(02)	0·978(04)	0·975(04)	0·971(06)	0·977(04)	0·963(02)

Experiment:	Ma72	Ma79	Ma77	Ma42	Ma35	Ma84	Ma27	Ma69	Ma24	Ma73	Ma70	Ma37	Ma39	Ma51	JK16*
Bulk comp.:	3	4	1	1	1	1	1	1	1	1	1	1	1	1	1
P (GPa):	4·0	4·0	4·5	5·0	6·0	7·0	7·5	8·0	8·5	8·0	8·0	4·0	4·0	4·0	3·0
T (°C):	1100	1100	1100	1100	1100	1100	1100	1100	1100	1200	1300	1000	900	800	1100
No. of analyses:	5	10	8	7	11	10	10	8	6	8	4	8	11	8	3
SiO_2	44·04(17)	45·15(23)	44·00(40)	44·71(45)	43·72(34)	43·33(29)	43·92(22)	44·22(24)	43·90(35)	44·47(58)	44·94(70)	43·65(30)	43·75(24)	43·22(34)	50·60(69)
Al_2O_3	12·60(23)	10·58(22)	12·14(15)	12·33(11)	12·44(13)	12·18(08)	12·13(07)	12·20(13)	11·80(08)	12·13(19)	12·02(23)	12·47(10)	12·39(08)	12·34(13)	8·79(47)
MgO	29·08(23)	28·03(25)	28·74(34)	28·92(14)	29·05(23)	28·84(35)	28·97(14)	28·80(19)	28·84(27)	28·68(39)	28·74(49)	28·77(15)	29·02(21)	28·98(24)	26·24(39)
CaO	<0·05	<0·05	<0·05	<0·05	<0·05	<0·05	<0·05	0·06(02)	0·06(04)	<0·05	0·13(04)	0·07(03)	<0·05	<0·05	<0·05
Na_2O	0·38(03)	0·05(01)	0·18(03)	0·15(04)	0·12(02)	0·10(02)	0·13(02)	0·10(02)	0·11(02)	0·07(02)	0·11(03)	0·14(02)	0·17(06)	0·11(03)	0·21(01)
K_2O	10·12(11)	11·04(15)	10·96(09)	10·67(15)	10·87(06)	10·92(10)	11·01(16)	10·92(16)	10·74(28)	10·86(13)	10·74(14)	10·86(18)	11·12(16)	10·90(14)	10·87(23)
H_2O	4·38(02)	4·30(02)	4·35(03)	4·40(03)	4·36(03)	4·32(03)	4·35(01)	4·36(02)	4·33(03)	4·37(05)	4·39(05)	4·35(02)	4·36(02)	4·33(02)	4·44(03)
Σ	100·63(35)	99·20(45)	100·39(78)	101·21(60)	100·60(54)	99·74(57)	100·55(25)	100·66(45)	99·77(84)	100·60(97)	101·07(117)	100·31(51)	100·85(33)	99·90(73)	101·15(84)
Si	3·017(07)	3·145(18)	3·035(14)	3·049(13)	3·009(09)	3·011(11)	3·026(09)	3·038(07)	3·045(11)	3·055(15)	3·069(20)	3·011(09)	3·009(11)	3·000(04)	3·415(42)
Al	1·017(16)	0·869(17)	0·987(08)	0·991(06)	1·009(11)	0·998(10)	0·985(07)	0·988(09)	0·964(08)	0·982(15)	0·967(26)	1·014(09)	1·004(06)	1·009(08)	0·699(37)
Mg	2·969(24)	2·910(19)	2·954(24)	2·939(22)	2·980(16)	2·987(23)	2·975(13)	2·950(16)	2·979(13)	2·936(23)	2·926(21)	2·959(11)	2·975(18)	2·997(09)	2·639(30)
Ca	—	—	—	—	—	—	—	0·005(02)	0·004(03)	—	0·010(03)	0·005(02)	—	—	—
Na	0·051(04)	0·007(02)	0·024(03)	0·020(05)	0·017(02)	0·014(02)	0·017(03)	0·013(03)	0·015(03)	0·010(02)	0·014(03)	0·019(03)	0·023(08)	0·015(05)	0·028(01)
K	0·885(11)	0·981(12)	0·964(11)	0·928(13)	0·955(08)	0·968(08)	0·967(14)	0·958(15)	0·945(20)	0·952(17)	0·936(04)	0·956(15)	0·976(16)	0·965(11)	0·936(13)
Σ	7·938(14)	7·912(18)	7·964(17)	7·927(18)	7·969(09)	7·978(14)	7·970(14)	7·946(13)	7·948(16)	7·933(16)	7·913(10)	7·960(13)	7·987(21)	7·986(08)	7·717(27)
K/(K+Na)	0·946(04)	0·993(02)	0·976(03)	0·979(05)	0·983(02)	0·986(02)	0·983(03)	0·987(03)	0·985(03)	0·990(02)	0·985(03)	0·981(03)	0·978(07)	0·985(05)	0·971(01)

Phlogopite formulae recalculated to 11 oxygens + stoichiometric OH.

Table 5: Average analyses of clinopyroxenes from high-pressure experiments

Experiment:	JK12	JK27	JK25	JK23	Ma31	Ma34	Ma20	Ma71	Ma72	Ma79	Ma77	Ma42	Ma35	Ma84	Ma27	Ma69
Bulk comp.:	1	1	1	1	1	1	1	2	3	4	1	1	1	1	1	1
P (GPa):	1·0	1·5	2·0	3·0	4·0	4·0	4·0	4·0	4·0	4·0	4·5	5·0	6·0	7·0	7·5	8·0
T (°C):	900	900	900	1000	1100	1200	1250	1100	1100	1100	1100	1100	1100	1100	1100	1100
No. of analyses:	12	10	10	10	13	10	7	6	5	10	10	13	7	10	7	5
SiO_2	55·79(37)	56·15(32)	56·31(24)	56·23(35)	56·54(35)	56·81(30)	56·19(55)	56·72(18)	57·01(11)	55·79(37)	56·20(26)	56·72(22)	56·25(53)	56·25(27)	56·19(54)	56·64(13)
Al_2O_3	1·12(41)	0·35(06)	0·65(18)	0·78(21)	1·74(52)	1·89(30)	1·18(23)	1·87(21)	2·92(17)	0·29(10)	1·08(16)	2·18(41)	2·85(26)	2·98(19)	3·27(23)	4·08(21)
MgO	18·26(44)	18·76(12)	18·55(20)	18·63(34)	18·00(59)	18·93(30)	19·22(48)	18·60(39)	17·81(32)	19·67(30)	18·70(22)	17·88(47)	17·71(31)	17·58(19)	17·45(44)	16·52(19)
CaO	25·27(39)	25·76(10)	25·55(44)	25·42(30)	23·68(42)	22·77(24)	24·19(64)	22·92(23)	22·27(25)	24·00(22)	24·43(23)	23·63(34)	22·65(44)	22·23(36)	21·78(16)	21·11(29)
Na_2O	0·72(21)	0·29(04)	0·52(18)	0·62(13)	1·20(29)	1·24(18)	0·73(12)	1·32(24)	1·84(16)	0·23(06)	0·86(08)	1·50(24)	1·84(16)	1·90(11)	2·11(16)	2·68(21)
K_2O	0·13(06)	0·14(04)	0·10(02)	0·11(04)	0·21(07)	0·13(06)	0·13(05)	0·13(05)	0·12(07)	0·22(03)	0·35(08)	0·16(04)	0·13(01)	0·12(03)	0·27(08)	0·33(04)
Σ	101·29(41)	101·45(37)	101·69(37)	101·78(66)	101·39(43)	101·77(40)	101·65(65)	101·56(33)	101·97(16)	100·19(41)	101·62(35)	102·07(37)	101·43(69)	101·06(49)	101·08(67)	101·37(21)
Si	1·984(07)	1·996(04)	1·995(04)	1·990(05)	2·000(06)	1·995(05)	1·985(07)	1·997(02)	1·995(02)	1·999(04)	1·990(04)	1·992(04)	1·984(04)	1·989(04)	1·986(04)	1·993(05)
Al	0·047(17)	0·015(02)	0·027(07)	0·029(06)	0·073(22)	0·078(12)	0·049(10)	0·078(09)	0·120(07)	0·012(04)	0·045(07)	0·090(17)	0·119(10)	0·124(08)	0·136(11)	0·169(09)
Mg	0·968(22)	0·989(04)	0·976(08)	0·987(11)	0·949(32)	0·991(15)	1·012(28)	0·976(19)	0·929(17)	1·050(14)	0·987(10)	0·936(25)	0·931(14)	0·926(07)	0·919(21)	0·866(11)
Ca	0·963(16)	0·981(05)	0·970(18)	0·966(07)	0·897(17)	0·857(09)	0·915(23)	0·865(08)	0·835(10)	0·921(12)	0·927(10)	0·889(13)	0·856(21)	0·842(15)	0·825(07)	0·796(12)
Na	0·050(14)	0·020(02)	0·036(12)	0·040(08)	0·082(20)	0·084(12)	0·050(08)	0·090(16)	0·125(11)	0·016(04)	0·059(05)	0·102(16)	0·126(11)	0·131(07)	0·145(12)	0·183(14)
K	0·006(03)	0·006(02)	0·005(01)	0·004(02)	0·010(03)	0·006(03)	0·006(02)	0·006(02)	0·006(03)	0·010(01)	0·017(03)	0·009(04)	0·006(01)	0·006(02)	0·012(04)	0·015(02)
Σ	4·017(06)	4·009(04)	4·011(05)	4·017(07)	4·011(05)	4·011(05)	4·017(09)	4·012(03)	4·009(03)	4·008(04)	4·025(07)	4·017(06)	4·022(04)	4·017(04)	4·023(07)	4·021(08)

Experiment:	Ma24	Ma73	Ma70	Ma74	Ma37	Ma39	Ma51
Bulk comp.:	1	1	1	1	1	1	1
P (GPa):	8·5	8·0	8·0	8·0	4·0	4·0	4·0
T (°C):	1100	1200	1300	1400	1000	900	800
No. of analyses:	8	11	10	6	11	19	8
SiO_2	56·41(55)	56·35(32)	57·17(13)	56·83(40)	56·51(40)	56·74(27)	56·25(48)
Al_2O_3	4·88(70)	4·02(25)	4·70(37)	4·34(12)	1·99(53)	1·80(69)	0·75(32)
MgO	16·57(65)	17·25(44)	18·16(76)	20·23(50)	18·08(51)	17·88(52)	18·70(48)
CaO	20·13(67)	20·80(65)	18·72(34)	17·39(36)	23·64(46)	24·11(59)	25·20(45)
Na_2O	2·98(41)	2·50(14)	2·74(26)	2·37(05)	1·29(29)	1·18(39)	0·53(21)
K_2O	0·30(07)	0·20(06)	0·35(11)	0·27(04)	0·12(03)	0·22(06)	0·15(02)
Σ	101·27(51)	101·12(56)	101·86(32)	101·42(46)	101·63(54)	101·94(38)	101·58(59)
Si	1·981(08)	1·985(05)	1·987(05)	1·978(05)	1·992(07)	1·998(05)	1·993(07)
Al	0·202(29)	0·167(10)	0·192(15)	0·178(04)	0·083(22)	0·075(30)	0·031(13)
Mg	0·868(35)	0·905(21)	0·941(39)	1·043(20)	0·950(26)	0·951(32)	0·988(23)
Ca	0·758(27)	0·785(26)	0·697(13)	0·648(16)	0·893(17)	0·910(24)	0·957(21)
Na	0·203(27)	0·171(10)	0·185(18)	0·160(03)	0·088(20)	0·081(27)	0·037(15)
K	0·013(03)	0·009(03)	0·016(05)	0·012(02)	0·006(01)	0·010(03)	0·007(01)
Σ	4·024(08)	4·021(05)	4·017(07)	4·019(07)	4·011(06)	4·010(04)	4·013(06)

Clinopyroxene formulae recalculated to 6 oxygens.

Table 6: Average analyses of garnets from high-pressure experiments

Experiment:	Ma73	Ma74
Bulk comp.:	1	1
P (GPa):	8·0	8·0
T (°C):	1300	1400
No. of analyses:	6	5
SiO_2	45·26(22)	45·67(33)
Al_2O_3	23·97(27)	23·97(19)
MgO	26·43(20)	27·76(37)
CaO	5·82(20)	4·34(33)
Na_2O	0·13(02)	0·11(02)
Σ	101·61(20)	101·85(59)
Si	3·038(12)	3·046(07)
Al	1·897(22)	1·885(06)
Mg	2·644(18)	2·761(19)
Ca	0·419(14)	0·310(25)
Na	0·017(02)	0·013(02)
Σ	8·014(03)	8·015(03)
Ca/(Ca + Mg)	0·137(05)	0·101(09)

Garnet formulae recalculated to 12 oxygens.

owing to the reaction $Mg_3Al_2Si_3O_{12}$ + $MgSiAl_{-2}$ = $Mg_3(MgSi)Si_3O_{12}$. The average Si values at 8·0 GPa and 1300°C (Kr-field II) and 8·0 GPa and 1400°C are 3·04 ± 0·01 (n = 6) and 3·05 ± 0·01 (n = 5), respectively. Owing to the small Si excess, a contribution from analytical errors cannot be ruled out. Constant small amounts of Na in garnet can be attributed to an Na-garnet component [$Ca_3Al_2Si_3O_{12}$ + $NaSiCa_{-1}Al_{-1}$ = $NaCa_2AlSi_4O_{12}$ (Ringwood & Major, 1971)]. Averaged garnet analyses are given in Table 6.

PHASE RELATIONS OF THE K-RICHTERITE + PHLOGOPITE + CLINOPYROXENE ASSEMBLAGE

In MARID-type assemblages (i.e. without olivine, orthopyroxene or garnet) there are insufficient phases to buffer the major exchange vectors among mica, amphibole and clinopyroxene. With the appearance of rutile and ilmenite, which are to a first approximation pure TiO_2 and pure $FeTiO_3$, the addition of Fe and Ti to the MARID bulk composition does not change the variance of the system. Therefore, we can consider the Fe–Ti absent subsystem KNCMASH a useful model system for MARIDs, uncomplicated by oxidation problems and even more complex substitutions involving Ti. The following vectors are buffered by exchange reactions between pairs of amphibole, mica and clinopyroxene:

KNa_{-1}	(kn)	amphibole, mica
$NaAl\square_{-1}Si_{-1}$	(ed)	amphibole, mica
$NaSiCa_{-1}Al_{-1}$	(pl)	amphibole, clinopyroxene
$Al_2Mg_{-1}Si_{-1}$	(tk)	amphibole, mica, clinopyroxene
$MgCa_{-1}$	(mc)	amphibole, clinopyroxene.

Following the method of Thompson *et al.* (1982), the MARID assemblage in the Kr-field I can be represented by three additive components: $\square Ca_2Mg_5Si_8O_{22}(OH)_2$ (TRE), $KMg_3AlSi_3O_{10}(OH)_2$ (PHL) and $CaMgSi_2O_6$ (DIO) for amphibole, mica and clinopyroxene, plus the exchange vectors listed above. For an open system, H_2O (in a fluid) will be an additional phase component. Additive components plus vectors allow a complete description of net-transfer and exchange reactions amongst amphibole, mica and clinopyroxene in the model system. Using the program REACTION (Finger & Burt, 1972) a total of five different net-transfer reactions as listed below can be formulated amongst the additive components and vectors chosen:

$$1\text{TRE} + \text{ed} + \text{kn} = \text{PHL} + 2\text{DIO} \quad (6)$$

$$6\text{TRE} + 2\text{ed} = 23\text{DIO} + 2\text{tk} + 2\text{pl} + 9\text{mc} + 6\text{H}_2\text{O} \quad (7)$$

$$23\text{PHL} = 11\text{TRE} + 19\text{ed} + 23\text{kn} + 4\text{pl} + 4\text{tk} + 18\text{mc} + 12\text{H}_2\text{O} \quad (8)$$

$$6\text{PHL} = 11\text{DIO} + 4\text{ed} + 6\text{kn} + 2\text{pl} + 2\text{tk} + 9\text{mc} + 6\text{H}_2\text{O} \quad (9)$$

$$2\text{PHL} + 4\text{TRE} = 19\text{DIO} + 2\text{kn} + 2\text{pl} + 2\text{tk} + 9\text{mc} + 6\text{H}_2\text{O}. \quad (10)$$

Of these five reactions only two are linearly independent. Vectors and additive components in reactions (6) and (7) can be combined to yield

$$\text{K-edenite} = \text{phlogopite} + 2\text{diopside} \quad (6a)$$

$$4\text{ tremolite} + 2\text{edenite} = 12\text{diopside} + 2\text{jadeite} + 9\text{enstatite} + 6\text{H}_2\text{O}. \quad (7a)$$

The slope of these reactions can be derived from thermodynamic data: even though these are poorly constrained for edenite (especially K-edenite) it is possible to obtain an order-of-magnitude estimate. Reaction (6a) yields a slope of 35–99 bar/K using phlogopite and diopside data from Holland & Powell (1990) and K-edenite data listed in Table 8. If the entropy of edenite given by Holland & Powell (1990) is used as a proxy for K-edenite the slope is flatter but still positive. Reaction (7a) has a negative slope of –105 to –72 bar/K between 1·0 and 4·0 GPa at 1100°C using the HSMRK equation of state of Delaney & Helgeson (1978) and solid-phase

Table 7: Representative mineral compositions for natural bulk composition AJE137

Experiment:	Ma2			Ma3				Ma4			Ma5				
P (GPa):	4·6			6·8				7·5			7·5				
T (°C):	1240			1345				1300			1200				
	opx	cpx	phl	opx	cpx	ga	ol	opx	cpx	ga	Kr	ga	phl	cpx	opx
SiO_2	57·71	54·37	40·94	57·00	55·69	42·07	40·42	56·10	54·23	42·04	54·28	41·75	45·03	55·00	58·66
TiO_2	0·19	0·42	2·92	0·30	0·33	2·66	<0·05	0·07	0·16	1·36	0·71	2·72	1·37	0·30	0·15
Al_2O_3	0·68	2·86	13·02	2·64	3·14	19·91	0·06	1·06	2·43	19·33	2·76	20·86	9·33	3·00	0·56
Cr_2O_3	<0·05	0·12	0·10	<0·05	<0·05	0·25	<0·05	<0·05	0·09	0·09	0·06	0·11	0·05	0·09	0·09
FeO*	5·13	4·57	4·22	2·18	3·39	5·61	5·91	2·95	3·08	5·32	4·00	6·58	5·71	6·41	3·63
MnO	0·05	0·05	<0·05	<0·05	0·06	<0·05	<0·05	<0·05	<0·05	<0·05	<0·05	0·08	<0·05	<0·05	0·06
MgO	34·96	19·22	22·37	33·43	23·24	21·93	50·65	35·22	20·60	24·68	20·69	16·91	22·94	16·20	36·43
NiO	n.d.	n.d.	n.d.	n.d.	n.d.	n.d.	n.d.	n.d.	n.d.	n.d.	0·34	0·10	0·70	0·28	0·20
CaO	0·71	15·14	0·22	2·82	11·29	6·46	0·10	1·36	15·76	5·08	5·70	8·61	0·01	14·34	0·94
Na_2O	0·18	1·85	0·11	0·55	1·50	0·09	0·05	0·25	1·72	0·08	2·81	1·00	0·05	3·38	0·16
K_2O	0·12	0·34	10·08	0·23	0·34	0·13	0·00	0·00	0·71	0·05	6·53	0·15	10·49	0·38	0·08
H_2O†			4·17								2·11		4·22		
Σ	99·70	98·89	98·16	99·15	98·98	99·11	97·34	97·05	99·60	98·03	99·99	98·87	99·92	99·38	100·96
Si	1·986	1·973	2·943	1·960	1·980	3·003	1·000	1·969	1·967	3·013	7·706	3·022	3·196	2·006	1·984
Ti	0·005	0·011	0·158	0·008	0·009	0·143	0·000	0·002	0·004	0·073	0·076	0·148	0·073	0·008	0·004
Al	0·028	0·122	1·103	0·107	0·132	0·014	0·002	0·044	0·104	1·633	0·461	1·78	0·780	0·129	0·023
Cr	—	0·004	0·006	—	—	0·014	—	—	0·003	0·005	0·007	0·006	0·003	0·003	0·002
Fe	0·148	0·139	0·254	0·063	0·101	0·335	0·122	0·086	0·093	0·319	0·475	0·399	0·339	0·196	0·103
Mn	0·002	0·002	—	—	—	—	—	—	—	—	—	0·005	—	—	0·002
Mg	1·793	1·040	2·396	1·714	1·232	2·333	1·868	1·843	1·114	2·636	4·377	1·825	2·427	0·881	1·837
Ni	—	—	—	—	—	—	—	—	—	—	0·039	0·006	0·04	0·008	0·005
Ca	0·026	0·589	0·017	0·104	0·430	0·494	0·003	0·051	0·613	0·39	0·868	0·668	0·001	0·560	0·034
Na	0·012	0·130	0·015	0·037	0·104	0·013	0·002	0·017	0·121	0·011	0·772	0·141	0·007	0·239	0·010
K	0·005	0·016	0·924	0·010	0·016	0·012	0·000	0·000	0·033	0·000	1·183	0·014	0·950	0·018	0·003
Σ	4·004	4·025	7·815	4·002	4·002	8·020	2·997	4·023	4·052	8·103	15·963	8·014	7·817	4·048	4·007
K/(K+Na)			0·984								0·605		0·993		
X_{Mg}	0·924	0·882	0·904	0·965	0·924	0·874	0·939	0·955	0·923	0·892	0·902	0·821	0·877	0·818	0·947

*Fe_{tot} = FeO. †Recalculation of mineral formulae assuming stoichiometric OH as in Tables 3–6. n.d., not determined.

Table 8: Thermodynamic data of amphiboles used in the present study to calculate the slope of reactions

		HP90	H78	K92	HS77
Edenite	V_0 (J/bar)	27·090	27·100	27·284	
	S_0 (J/mol K)	599·000	674·075	572·402	
K-edenite	V_0			27·370	27·91
	S_0			581·371	
Tremolite	V_0	27·270	27·292	27·176	
	S_0	550·000	549·266	553·979	

HP90, Holland & Powell (1990); H78, Helgeson *et al.* (1978); K92, Karzhavin (1992); HS77, Hinrichsen & Schürmann (1977).

data of Holland & Powell (1990). Reactions (6) and (8) involve kn + ed exchange between mica and amphibole transforming phlogopite to amphibole with increasing K/Na, which is consistent with the amphibole chemistry and calculated modes observed with increasing pressure.

The relation between bulk composition and phase composition in the model MARID system: experiments at different K/Na ratios

Natural MARID as well as MARI bulk compositions show a large variation in terms of K/Na ratios. Analyses by Waters (1987*a*) show that K/Na varies from 1·2 to 19·7, whereas values of $(K_2O + Na_2O)/Al_2O_3$ (the peralkalinity index, PI) show a smaller variation from ~1·1 to 2·0. To explore the range of bulk K/Na ratios that crystallize richteritic amphiboles and to investigate the variation of the mineral compositions with changing bulk composition, three additional oxide-mixtures were prepared with K/Na ratios of 1·0, 1·4 and 20·3 at a constant PI (Table 1). These span the whole range of bulk K/Na ratios for natural MARI(D)s given by Waters (1987*a*). The different bulk compositions are plotted in Fig. 13a–d on a $CaO–Na_2O–K_2O$ triangle with respect to the compositions of K-richterite, phlogopite and clinopyroxene. In Fig. 13d, bulk composition 4 plots very close to the clinopyroxene–phlogopite tie-line, which is expressed in a very small modal amount of amphibole in run Ma79. Bulk compositions with higher bulk K/Na ratios therefore would destabilize amphibole and give rise to a two-phase phlogopite + clinopyroxene assemblage. Bulk 3, on the other hand, produces much more clinopyroxene than expected from its position with respect to the phlogopite–K-richterite tie-line (Fig. 13b). This can be explained by the presence of substantial Al in clinopyroxene coupled to Na via jadeite solid solution. Al is not considered in the projection and stabilizes clinopyroxene relative to amphibole. Fig. 14 shows that in experiments at constant P and T phase chemistries show a systematic variation with changing bulk K/Na. The total K in amphibole exhibits a strong increase with increasing bulk K/Na (Fig. 14a). Runs Ma79 (4·0 GPa and 1100°C) and JK22 (3·0 GPa and 1000°C), both using the bulk composition 4, contain amphiboles with 1·19 ± 0·04 and 1·13 ± 0·01 ($n = 4$) K p.f.u. This demonstrates that significant amounts of K can enter the M(4)-site in bulk compositions with high K/Na, even at moderate pressures. With increasing bulk K/Na, Al drops from 0·60 p.f.u. in bulk 3 to 0·17 p.f.u. in bulk composition 4 (Fig. 14a).

With increasing bulk K/Na both coexisting phlogopite and clinopyroxene show a decrease in Na and Al. In clinopyroxene Na and Al are coupled in decreasing jadeite content. As a result of decreasing Na, X_K in phlogopite increases, as is shown in Fig. 14b, where $X_{K,phl}$ is plotted against $X_{K,amph}$. Figure 14c shows that increasing bulk K/Na promotes montdorite-exchange $\square Si_2Mg_{-1}Al(IV)_{-2}$ in phlogopite. This has implications for trace element partitioning, as an increase in the number of six-coordinated vacancies provides crystallographic sites for the accommodation of trace elements.

DISCUSSION

The K/Na ratio in amphibole and phlogopite and their molar volumes

In natural $C2/m$ amphiboles K is assigned exclusively to the 12-coordinated A-site, whereas Na can occupy the A-site and/or the eight-coordinated M(4)-site (Hawthorne, 1981). Huebner & Papike (1970) investigated cell parameters of richteritic amphiboles with different K/Na ratios synthesized at 0·1 GPa. They attributed the change in lattice parameters with decreasing K/Na to a progressive collapse of the A-site. This can be explained in terms of the difference in ionic radii between K and Na

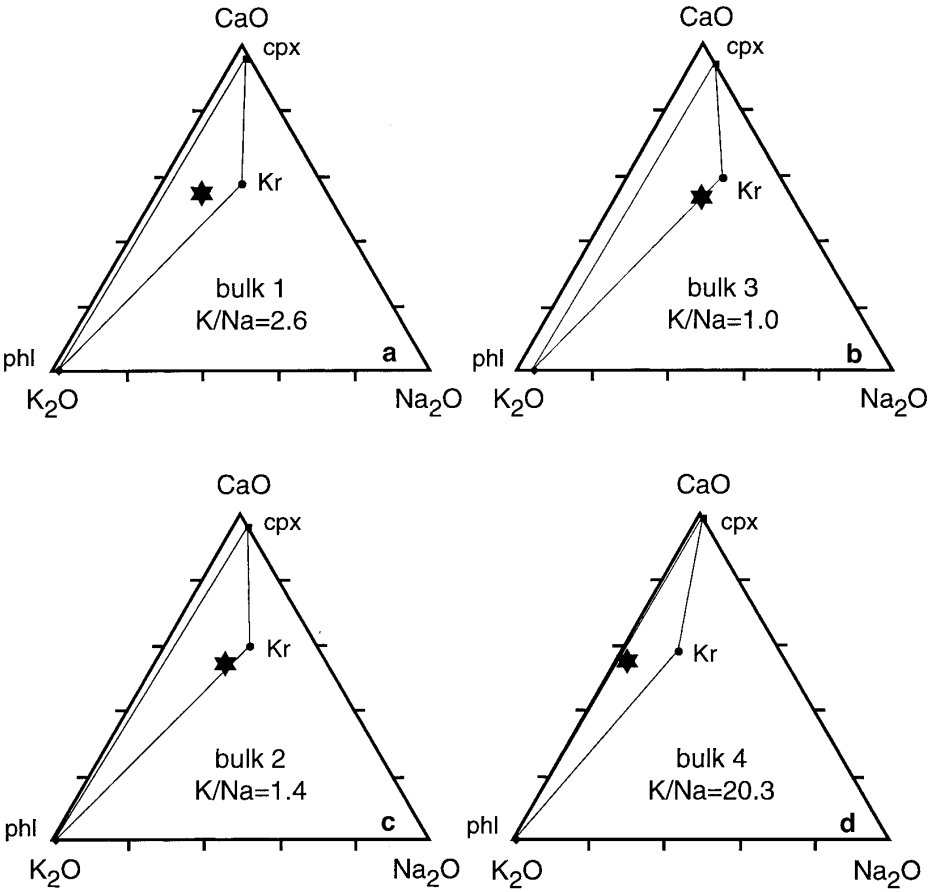

Fig. 13. Variation of bulk composition and mineral composition in the KNCMASH system shown in a molar CaO–K_2O–Na_2O compositional triangle for experiments conducted at 4 GPa and 1100°C. Black stars represent bulk compositions with different K/Na ratios (see Table 1). Averaged compositions of K-richterite, phlogopite and clinopyroxene are connected by tie-lines.

(1·64 for K compared with 1·39 for Na in 12-coordination; Shannon, 1976). It is because K is considerably larger than Na that the unit-cell volumes of richteritic amphiboles increase with increasing K/Na from 273·93 cm^3/mol for Na-richterite to 277·48 cm^3/mol for K-richterite (Huebner & Papike, 1970). Such an increase in unit-cell volume with increasing K/Na is therefore a common feature in alkali-bearing amphiboles, as observed in (Na,K)-pargasites and -edenites by Hinrichsen & Schürmann (1977).

In this study, K-richterites show a systematic increase in K and K/Na with increasing pressure. Such behaviour would not be expected from a consideration of simple molar volumes. Two possibilities for the preferential incorporation of K with increasing *P* have to be considered: (1) K increases the intrinsic stability of the amphibole structure at high pressure to an extent that outweighs the increase in molar volume; K fits into the A-site more tightly than does Na, such that K may support the lattice around the A-site and thus prevent a breakdown of the structure at high pressure. (2) K-richterite is involved in reactions that decrease the overall volume of the system, and this decrease compensates for the increase in molar volume of amphibole. Comodi *et al.* (1991) investigated the compressibility of tremolite, glaucophane and pargasite to 4·1 GPa and found very similar changes in unit-cell parameters for these amphiboles. Therefore, the reasons for glaucophane and not tremolite being the typical high-pressure amphibole are not related to different elastic properties, but rather to a reaction such as tremolite + albite = glaucophane + diopside + quartz. This reaction decreases the overall volume by ~8% and involves a transfer of tetrahedrally to octahedrally coordinated Al (Comodi *et al.* 1997). In the same way, the reaction

$$\text{phlogopite} + 2\text{diopside} = \text{K-edenite}$$

$$282{\cdot}02\ cm^3\ (\text{HP90}) = 279{\cdot}12\ cm^3\ (\text{HS77})$$

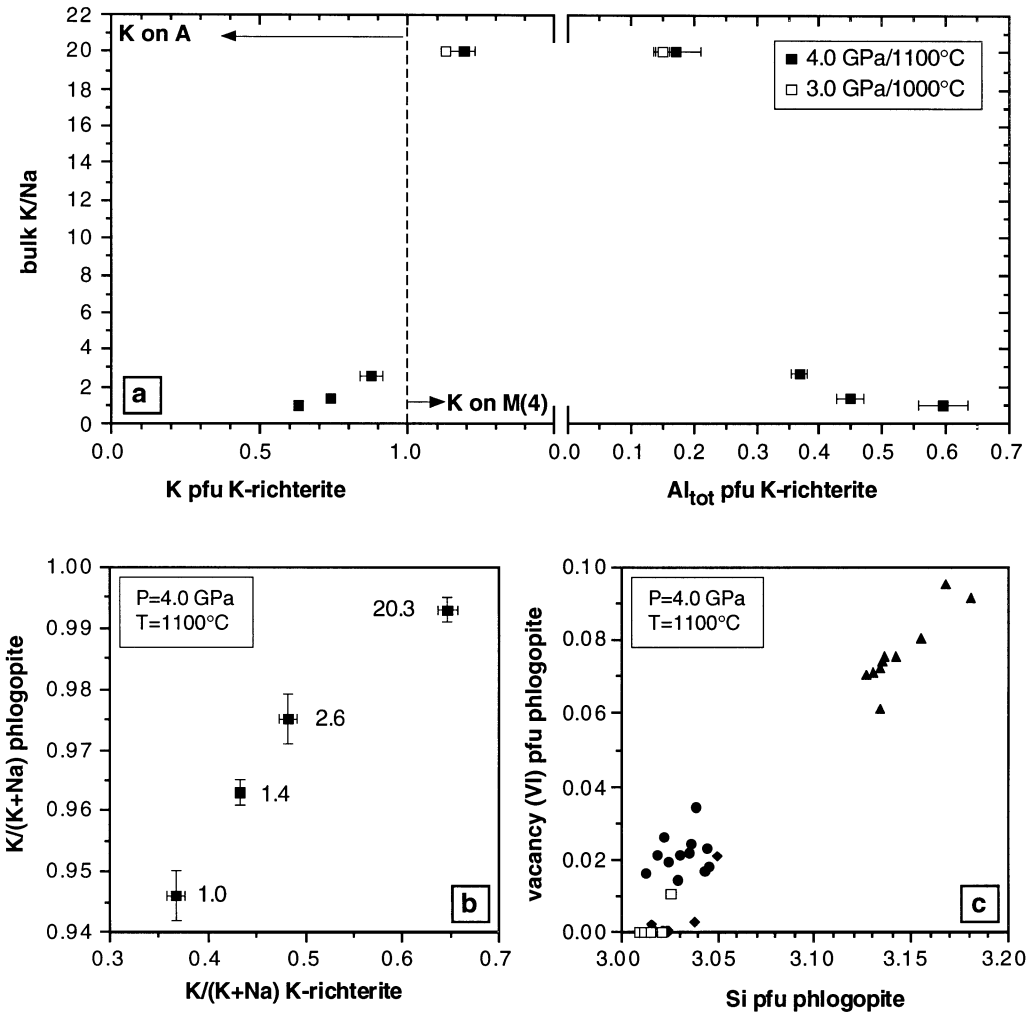

Fig. 14. (a) Variation of K-richterite composition as a function of the bulk K/Na ratio at constant *P* and *T*. Individual data points represent averaged values of 4–10 analyses (see Table 3). (b) Covariation of K/(K + Na) in K-richterite and coexisting phlogopite as a function of bulk K/Na ratio at constant *P* and *T*. Individual data points represent averaged values of 4–10 K-richterite analyses and 6–12 phlogopite analyses; numbers next to data points are bulk K/Na ratios. (c) Covariation of Si and six-coordinated vacancy p.f.u. in phlogopites as a function of bulk K/Na ratio at constant *P* and *T*; triangles, Ma79 with bulk K/Na 20·3; diamonds, Ma71 with bulk K/Na 1·4; circles, Ma31 with bulk K/Na 2·.6; squares, Ma72 with bulk K/Na 1·0 (see Tables 3 and 4).

[where HP90 is Holland & Powell (1990) and HS77 is Hinrichsen & Schürmann (1977)] transforming mica and clinopyroxene to amphibole results in an overall volume reduction of 1–3%: ΔV_s is between –2·9 and –8·3 cm^3/mol and is dependent on the molar volume of K-edenite (Table 8). This was already noted by Huebner & Papike (1970) and taken as an indication for preferential stabilization of potassic amphibole relative to clinopyroxene and phlogopite at high pressure. Similar considerations may be applied to K-richterite stability in subalkaline, opx-bearing systems where K-richterite and garnet are stabilized relative to pyroxene and phlogopite, through the reaction phlogopite + diopside + jadeite + 2enstatite = K-richterite + pyrope (Luth *et al.*, 1993). This reaction has a ΔV_s of –10·8 cm^3/mol, equivalent to a volume-reduction of ~2·7% (Holland & Powell, 1990). The increase in tk-exchange component in K-richterite and jadeite component in clinopyroxene observed in the present study is consistent with the conclusion of Comodi *et al.* (1991) and reflects increasing octahedral Al-coordination with increasing pressure. Comodi *et al.* (1991) showed that elastic properties of calcalkaline amphiboles are not significantly influenced by the degree of A-site occupancy. In view of this, it is

assumed that high-K amphiboles are stabilized at high pressure by reactions that reduce the overall volume of the system rather than by a change of elastic properties owing to K entry into the lattice.

In the absence of crystal-structure refinements for K-richterite with K >1·0 p.f.u., 'excess' K is assigned to the M(4)-site because this position is the second largest in the amphibole structure and has the second highest coordination number. Moreover, exchange of sodium by potassium on the A-site increases the dimensions of the octahedral strip as well as mean M(4)–O distances (Cameron *et al.*, 1983), thereby creating conditions favourable for the occupation of M(4) by a large ion.

Similar considerations are valid for phlogopite. Like K-richterite, (Na,K)-phlogopite shows an increase in molar volume with increasing KNa_{-1}.The volume difference between K-phlogopite (149·91 cm^3/mol; Robie *et al.*, 1978) and Na-phlogopite (144·47 cm^3/mol; Carman, 1974) is even larger than between potassic and sodic richterite. This led Arai (1986) to conclude that Na-phlogopite is stabilized with respect to K-phlogopite with increasing pressure. This is not supported by the present study, however, where the X_K in phlogopite slightly increases in both the natural and synthetic systems with increasing pressure. Therefore, directions of changes in composition with pressure must depend upon the ΔV of reactions involving the amphiboles and micas, not just such changes for the phases themselves.

K/Na in natural and synthetic K-richterites: some clues to MARID-suite petrogenesis

Amphiboles from MARID-suite xenoliths show a relatively restricted range in composition with respect to K/Na and K/(K + Na) ratios and usually small within-sample variations. With few exceptions, K/Na ratios of K-richterite range between ~0·75 and 1·05. Figure 15 shows a plot of the K/Na ratios of MARID-suite amphiboles vs. Mg/(Mg + Fe^{2+}) and Ti p.f.u., respectively. It is obvious that both Fe and Ti, which represent the most important components in K-richterites not considered in the present study, do not directly influence K/Na ratios of the amphiboles. All MARID-suite amphiboles examined from group I (basaltic) kimberlite localities have K <1·0 p.f.u. whereas amphiboles from the only known MARID occurrence in a group II (micaceous) kimberlite (orangeite), Newlands, mostly show K ≥1·0 pfu. K-richterite analyses from a Newlands sample yield an average K/Na of 1·224 ± 0·054 (n = 17) with K = 1·017 ± 0·020 and K(M4) = 0·041 ± 0·023 p.f.u. This is consistent with analyses reported by Dawson & Smith (1977) (sample BD1778) and Waters *et al.* (1989) (sample LD99). Whereas almost all synthetic K-richterites show total cation numbers very close to 16·0, natural K-richterites including Newlands amphiboles usually have

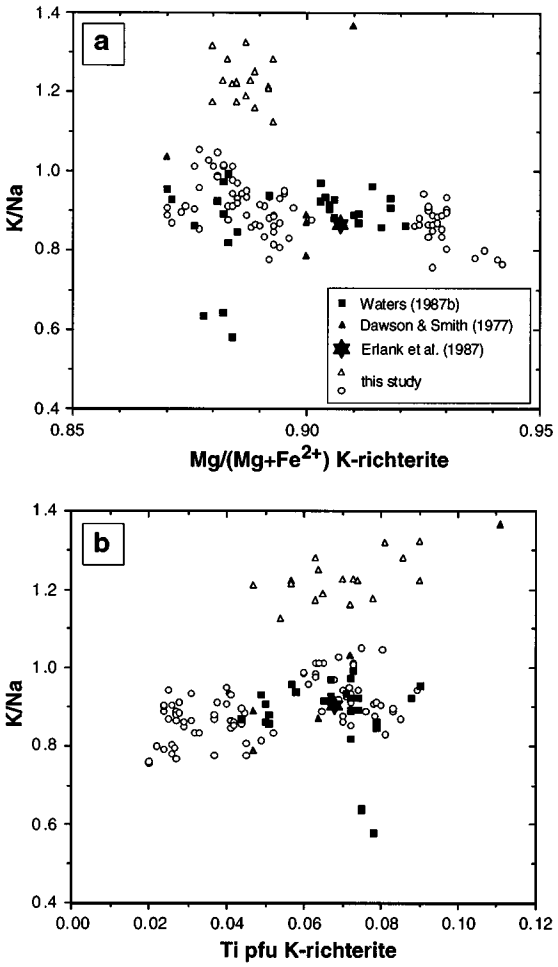

Fig. 15. K/Na ratio vs (a) Mg/(Mg + Fe^{2+}) and (b) Ti p.f.u. of K-richterites from natural MARID-type K-richterite–phlogopite–clinopyroxene assemblages. Source of data: squares, Waters (1987*b*); solid triangles, Dawson & Smith (1977); star, average of 53 K-richterite analyses from 10 MARID samples, Erlank *et al.* (1987). Additional amphibole data obtained for this study: open circles, data from 11 MARID xenoliths (Kimberley dumps, DeBeers collection); open triangles, K-richterite data from a Newlands (group II kimberlite) MARID xenolith (University of Cape Town Collection).

0·02–0·05 vacancies on the A-site p.f.u. when normalized to 24 oxygens. This might be an artefact of the normalization procedure that does not take into account potential ferric iron.

The restricted range in K/Na of amphiboles is in contrast to the wide variation in bulk K/Na ratios. Figure 16 shows a plot of bulk K/Na ratios vs corresponding K/Na ratios in K-richterites. There is no obvious correlation between bulk K/Na and K/Na in amphibole. In an incompletely buffered closed system, however, such a correlation should occur, as demonstrated by the experiments. MARID-suite rocks, therefore, do not represent the bulk system from which they formed, but are

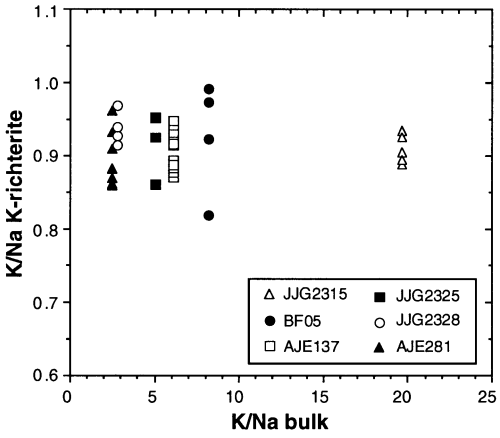

Fig. 16. K/Na ratio of bulk composition vs K/Na ratio of K-richterites. Bulk compositional data are from Waters (1987*a*, table 3, analyses 1–6), with K-richterite analyses from the same samples also from Waters (1987*b*). The bulk composition of AJE137 is from Sweeney *et al.* (1993).

products of an open-system crystallization. An open-system formation is also implicit in the suggestion by Dawson & Smith (1977), on the basis of textural arguments, that MARIDs are cumulates crystallized from a magma body, an opinion supported by Waters (1987*a*). Harte *et al.* (1993) devised a general open-system model for the formation of metasomatic dykes and veins by a process of crystal sorting and residue-deposition in a flowing fluid/melt, where the crystal aggregates do not represent the bulk melt compositions.

Experiments on the natural MARID composition AJE137 have shown that near-solidus partial melts are saturated in olivine and/or orthopyroxene over a significant pressure interval (4·5–7·5 GPa, Fig. 6). These phases are, with very few exceptions, not part of MARID-type assemblages. Interestingly, in the experiments on AJE137 with added water, conducted by Sweeney *et al.* (1993), olivine and orthopyroxene are absent under subsolidus conditions (see Fig. 6; Sweeney *et al.*, 1993), although they are present well above the solidus coexisting with a melt. We suggest that cooling and crystallization of a MARID parental liquid to conditions close to the solidus yields an extremely potassic and silica-rich liquid. On further cooling, the amount of crystallized olivine and orthopyroxene is reduced by peritectic reaction with the residual liquid to form amphibole and phlogopite. Eventually, a temperature condition is reached (near or sub solidus) where a fluid segregates and within which the small amounts of any remaining olivine and orthopyroxene may be partially or completely dissolved. In the system K_2O–Na_2O–FeO–MgO–CaO–Al_2O_3–SiO_2–TiO_2–H_2O a near-solidus assemblage K-richterite + phlogopite + clinopyroxene + orthopyroxene + olivine + ilmenite + rutile + liquid + vapour would be completely buffered, but the disappearance of olivine + orthopyroxene + liquid would result in a loss of complete buffering for subsolidus MARID assemblages. The MARID bulk composition parental to AJE137 has thus been modified by at least incongruent dissolution effects. Experiments (see above) demonstrate that near-solidus or subsolidus fluids are highly charged with alkalis, Mg, Al and Si, and are capable of storing a substantial part of the alkali budget of MARID-type bulk systems. These solute-charged fluids may leave the system continuously along chemical or P–T gradients either during or after the dyke or vein formation.

The experiments show that the pressure effect on K/Na and X_K of amphibole is small compared with the influence of the bulk composition. If MARIDs formed from bulk compositions with strongly variable bulk K/Na ratios, this should be expressed as a wide range of K/Na amphibole ratios. The limited range of K/Na encountered in MARID amphiboles from group I occurrences, however, suggests a formation in an environment with relatively constant K/Na ratios. Owing to the positive correlation between K/Na_{amph} and K/Na_{bulk}, the K-rich K-richterites from Newlands MARIDs formed either under unusually high pressure or in a bulk system with unusually high K/Na compared with group I occurrences.

A possible origin for MARIDs

We suggest two mechanisms which may explain the origin of MARIDs in regions of the mantle associated with thermal plumes. First, MARIDs may be a high-potassic liquid derived from great depths (eventually from within the diamond stability field), equilibrated with a peridotite and intruded to high levels through crack propagation. Alternatively, MARIDs may derive from group II kimberlites (orangeites) as a residual liquid resulting from the fractionation of olivine and exsolution of a carbonatitic component (Sweeney *et al.*, 1993). It is noteworthy that some evolved group II kimberlites contain K-richterites very similar in chemistry to MARID amphiboles (Mitchell, 1995*b*). Compared with the primitive group II rocks that are rich in MgO, P_2O_5, K_2O and carbonate, evolved varieties are enriched in SiO_2 and Al_2O_3, and depleted in MgO and carbonate. Such differences could indeed be explained by a trend involving olivine fractionation and carbonatite exsolution. Clearly, any petrogenetic relationship between group II kimberlite magmatism and MARIDs implies a secular relationship. Such a relationship is suggested by the dating of MARID zircons by Konzett *et al.* (1995).

Stability of MARID-type assemblages in continental lithosphere

Sweeney *et al.* (1993) studied the phase relations of a natural MARID assemblage up to 3·5 GPa. These workers showed that only H_2O-rich ($\geq$10 wt % H_2O) melts derived from MARIDs crystallize K-richterite above the solidus, a prerequisite to explain the amphibole-involved cumulate textures often observed in natural MARIDs. The solidus of these H_2O-rich melts intersects a 40 mW/m^2 shield geotherm beneath the Kaapvaal Craton (Pollack & Chapman, 1977) between 3 and 4 GPa (Fig. 6), which represents an upper pressure limit for MARID stability under these conditions. The solidus of MARID compositions with lowered water content is shifted towards considerably higher temperatures (Fig. 6). In this case, melts would crystallize K-richterite from the very last batch of melt and no cumulate textures would occur.

Lithospheric P–T conditions for the Kaapvaal Craton derived from garnet peridotite suites show a considerable scatter in their trends (see Fig. 6), which is, at least in part, due to different geothermobarometer calibrations used in various studies (Berrand & Mercier, 1985; Bertrand *et al.*, 1986; Finnerty & Boyd, 1987; Waters & Erlank, 1988; Phillips & Harris, 1995). Evaluation of different geothermobarometers is beyond the scope of this paper, and some generalizations concerning the stability of MARID-type assemblages are still possible in the absence of consistent P–T estimates. In continental lithosphere governed by a 40 mW/m^2 geotherm, MARIDs are stable to ~6 GPa, and in cooler mantle regions, such as those indicated by diamond inclusion data from xenoliths of the Kimberley area (Phillips & Harris, 1995; Fig. 6), they can persist to even higher pressures. In lithospheric mantle with T displaced from the 40 mW/m^2 geotherm towards higher values (e.g. northern Lesotho, Fig. 6) MARIDs will start melting by decompression without additional input of heat at P <6 GPa.

The experiments in this study show that K-richterite and phlogopite have increasing X_K and K/Na ratios with increasing pressure and will produce partial melts with increasing K/Na. This occurs because near-solidus melts are dominated by incongruent melting of K-richterite according to K-richterite = enstatite + diopside + L, or K-richterite = olivine + diopside + L (Sweeney *et al.*, 1993), and also because subsolidus reactions increase K/Na through consumption of phlogopite. Increasing solubility of jadeite component in clinopyroxene will enhance this effect at high pressures. In F- and Ti-rich systems, solid-solution effects will prevent rapid elimination of amphibole and result in the formation of partial melts coexisting with increasingly F- and Ti-rich amphibole and phlogopite residua over a large T interval (Forbes & Flower, 1974; Foley, 1991).

The experiments using AJE137 demonstrate that at $P \geq 4{\cdot}6$ GPa low-degree MARID partial melts (run ma2 in Fig. 6) are not in equilibrium with garnet- or olivine-bearing mantle. At higher degrees of partial melting, however, MARID melts of this bulk composition become saturated in the garnet lherzolite assemblage garnet + orthopyroxene + clinopyroxene + olivine (e.g. run ma1).

MARID-type assemblages are clearly stable within the diamond stability field and K-richterite + garnet is a potentially stable high-pressure assemblage not only in subalkaline peridotitic systems (Trønnes *et al.*, 1988), but also in Al-poor MARID bulk systems. Several lines of evidence support the co-stability of K-richterite with diamond. For example, Leung *et al.* (1994) reported polyphase inclusions in diamond from Fuxian, China, comprising diopside + biotite + rutile, diopside + apatite + rutile and, more unusually, garnet + biotite + apatite + rutile. Although the mica is unusually rich in Fe the assemblages are typical for the MARID suite. It is noteworthy that one inclusion assemblage is olivine + clinopyroxene + amphibole, the latter being most likely K-richterite (I. S. Leung, personal communication, 1995). The coexistence with olivine and the relatively Ti-poor and Cr-rich composition of K-richterite (I. S. Leung, unpublished data, 1995), however, makes a peridotitic (or PKP) origin of this amphibole more likely. Phlogopite + K-richterite with the typical MARID chemical signature has been described as a diamond inclusion from the Sloan Kimberlite, Colorado, by Meyer & McCallum (1986). Although these workers considered K-richterite to be an epigenetic inclusion, it has to be noted that K-richterite is not considered a stable phase in group I kimberlites (see Mitchell, 1995*b*). Thus, it is difficult to envisage a process by which K-richterite is trapped on the diamond's way to the surface. MARID stability within the diamond field also provides a link to the extremely potassic melt–fluid inclusions in diamond which are characterized by high K_2O/Al_2O_3 and K_2O/Na_2O ratios (Navon *et al.*, 1988; Schrauder & Navon, 1994).

Amphibole stability in peralkaline vs subalkaline bulk compositions

The experiments of this study underline the fundamental difference between peralkaline and subalkaline bulk compositions with respect to amphibole stability. Alkali-amphiboles are continuously stable from low-P(T) crustal environments (e.g. Velde, 1978) to at least 8·5 GPa in peralkaline systems and are thus available as a low-melting component and source of H_2O and alkalis during melt formation (Foley, 1992; Sweeney *et al.*, 1993; Van der Laan & Foley, 1994). The extreme stability of alkali-amphiboles is due to their strong variability in K/Na

ratios and a high-pressure assemblage usually containing phlogopite + clinopyroxene that favours amphibole stability with increasing pressures. Subalkaline (or peridotitic) systems, on the other hand, are characterized by a stability gap between ~3 and 6 GPa. Below 3 GPa, pargasitic and/or kaersutitic amphiboles are widespread in metasomatically altered peridotites (Green, 1973; Green & Ringwood, 1967; Millhollen *et al.*, 1974; Merrill & Wyllie, 1975; Mysen & Boettcher, 1975, 1976; Mengel & Green, 1989; Wallace & Green, 1991) and may be principal hosts of alkalis, water and a number of incompatible trace elements in shallow-level peridotites (O'Reilly *et al.*, 1991; Ionov & Hofmann, 1995). Above ~6 GPa, K-amphibole can be stable in peridotites as a product of phlogopite breakdown (Trønnes *et al.*, 1988; Sudo & Tatsumi, 1990). K-amphibole from these environments may control the composition of coexisting hydrous fluids in subduction zones (Tatsumi *et al.*, 1991; Tatsumi & Eggins, 1995). At pressures above Ca-amphibole-out and below K-amphibole-in, phlogopite is the only stable hydrous silicate phase.

CONCLUSIONS

Experiments in the KNCMASH system show that the typical MARID assemblage K-richterite + phlogopite + clinopyroxene is stable over a wide P range up to at least 8·5 GPa at T <1400°C. Temperatures of K-richterite breakdown vary from 1135–1200°C at 4·0 GPa to 1300–1400°C at 8·0 GPa in runs with 4·7 wt % H_2O added. K-richterite breaks down at or slightly below the solidus. Observed phase relations are consistent with an incongruent melting of K-richterite to form clinopyroxene + olivine + liquid. MARIDs are stable far into the diamond stability field and MARID-suite phases may be trapped as primary inclusions in diamonds. Other evidence is provided by polyphase inclusions of MARID-suite minerals reported from Chinese diamonds (Leung *et al.*, 1994) and by a K-richterite + phlogopite inclusion described by Meyer & McCallum (1986).

At 8·0 GPa and 1300°C, K-richterite coexists with garnet + phlogopite + olivine + clinopyroxene in the KNCMASH system. The garnet + K-richterite stability field has a narrow P–T range at P >7·0 GPa and 1200<T<1400°C. Phase relations of natural MARID AJE137 are consistent with those in the synthetic system and confirm the potentially stable coexistence of K-richterite + garnet at high P (and T) not only in subalkaline, peridotitic systems (Trønnes *et al.*, 1988), but also in strongly peralkaline, Al-poor environments.

All amphiboles synthesized in the present study are classified as K-richterites. In a given bulk composition the most important change in amphibole chemistry is an increase in the overall K/(K + Na) ratio with increasing pressure. In a bulk composition with molar K/Na = 2·6, amphiboles do not incorporate significant amounts of K(M4) up to 8·5 GPa and 1200°C but approach values of K/(K + Na) on the A-site of 1·0. The appearance of garnet at 8·0 GPa and 1300°C causes a drastic increase in K with significant K on M(4). Amphiboles with KKCa component coexisting with garnet were also encountered in natural MARID AJE137. All K-richterites contain small amounts of Al both as Al(IV) and Al(VI). With increasing pressure, Al increases systematically along with a slight decrease in Ca. An isobaric section at 4·0 GPa shows that T variation does not significantly affect X_K and only slightly influences Al and Ca. Clinopyroxenes coexisting with K-richterite show a regular increase in jadeite component with increasing P. The nearly 1:1 correlation between Al and Na precludes any significant Ca-Tschermaks component. Coexisting phlogopite shows the least variability with a slight increase in K/(K + Na) and minor variation in Al. Garnet first appears at 8·0 GPa and 1300°C; it shows a minor grossular and a small majorite component.

K-richterites are stable in an extremely wide range of bulk K/Na ratios. As the assemblage K-richterite + phlogopite + clinopyroxene is incompletely buffered within the KNCMASH system, experimentally grown K-richterites show a systematic variation in their K/Na ratios with changing bulk K/Na. Most importantly, K-richterites can accommodate significant amounts of K(M4) even at moderate pressures, provided the bulk K/Na ratio is sufficiently high. As opposed to the experimental results, natural MARID amphiboles and clinopyroxenes do not show the systematic interrelation between bulk and mineral chemistry as expected in an incompletely buffered system. We explain this absence of a systematic relation in amphibole (and clinopyroxene) chemistry in the natural system by open-system crystallization. The absence of olivine and orthopyroxene from natural MARID assemblages is explained by a peritectic removal of these phases under near-solidus conditions.

We suggest two mechanisms which may explain the origin of MARIDs in regions of the mantle associated with thermal plumes. First, MARIDs may be a high potassic liquid derived from great depths (eventually from within the diamond stability field), equilibrated with a peridotite and intruded to high levels through crack propagation. Alternatively, MARIDs may derive from group II kimberlites (orangeites) as a residual liquid resulting from the fractionation of olivine and exsolution of a carbonatitic component (Sweeney *et al.*, 1993).

ACKNOWLEDGEMENTS

Mike Skinner and John Bristow are thanked for the generous permission to take MARID samples from the

DeBeers collection. Karen Olson kindly provided a MARID sample from the Newlands kimberlite. Irene Leung is thanked for providing unpublished data on metasomatic diamond inclusions, and Eric Reusser for a computer program to calculate modal amounts of minerals. Thoughtful and constructive reviews by Alison Pawley and Steven Foley are gratefully acknowledged. This work was supported by the Swiss National Science Foundation.

REFERENCES

Aoki, K., 1975. Origin of phlogopite and potassic richterite-bearing peridotite xenoliths from South Africa. *Contributions to Mineralogy and Petrology* **53,** 145–156.

Arai, S., 1986. K/Na variation in phlogopite and amphibole of upper mantle peridotites due to fractionation of the metasomatising fluids. *Journal of Geology* **94,** 436–444.

Barton, M. & Hamilton, D. L., 1982. Water-undersaturated melting experiments bearing upon the origin of potassium-rich magmas. *Mineralogical Magazine* **45,** 267–278.

Bertrand, P. & Mercier, J.-C. C., 1985. The mutual solubility of coexisting ortho- and clinopyroxene: toward an absolute geothermometer for the natural system. *Earth and Planetary Science Letters* **76,** 109–122.

Bertrand, P., Sotin, C., Mercier, J.-C. C. & Takahashi, E., 1986. From the simplest chemical system to the natural one: garnet peridotite barometry. *Contributions to Mineralogy and Petrology* **93,** 168–178.

Bohlen, S. R., Essene, E. J. & Boettcher, A. L., 1980. Reinvestigation and application of olivine–qtz–opx-barometry. *Earth and Planetary Science Letters* **47,** 1–10.

Bose, K. & Ganguly, J., 1995. Quartz–coesite transition revisited: reversed experimental determination at 500–1200°C and retrieved thermochemical data. *American Mineralogist* **80,** 231–239.

Brey, G. P. & Köhler, T., 1990. Geothermobarometry in four-phase lherzolites II. *Journal of Petrology* **31,** 1353–1378.

Cameron, M., Sueno, S., Papike, J. J. & Prewitt, C. T., 1983. High temperature crystal chemistry of K and Na fluor-richterites. *American Mineralogist* **68,** 924–943.

Carman, J. H., 1974. Synthetic sodium phlogopite and its two hydrates: stabilities, properties, and mineralogical implications. *American Mineralogist* **59,** 261–273.

Comodi, P., Mellini, M., Ungaretti, L. & Zanazzi, P. F., 1991. Compressibility and high pressure structure refinement of tremolite, pargasite and glaucophane. *European Journal of Mineralogy* **3,** 485–499.

Cundari, A., 1973. Petrology of the leucite-bearing lavas in New South Wales. *Journal of the Geological Society of Australia* **20,** 465–491.

Dawson, J. B. & Smith, J. V., 1977. The MARID (mica–amphibole–rutile–ilmenite–diopside) suite of xenoliths in kimberlite. *Geochimica et Cosmochimica Acta* **41,** 309–323.

Delaney, J. M. & Helgeson, H. C., 1978. Calculation of the thermodynamic consequences of dehydration in subducting oceanic crust to 100 kb and >800°C. *American Journal of Science* **278,** 638–686.

Della Ventura, G., Maras, A. & Parodi, G. C., 1983. Potassium-fluor-richterite from Monte Somma (Campania, Italy). *Periodico di Mineralogia* **52,** 617–630.

Edgar, A. D. & Vukadinovic, D., 1993. Potassium-rich clinopyroxene in the mantle: an experimental investigation of a K-rich lamproite up to 60 kbar. *Geochimica et Cosmochimica Acta* **57,** 5063–5072.

Edgar, A. D., Charbonneau, H. E. & Mitchell, R. H., 1992. Phase relations in an armalcolite–phlogopite lamproite from Smoky Butte, Montana: applications to lamproite genesis. *Journal of Petrology* **33,** 505–520.

Erlank, A. J. & Finger, L. W., 1970. The occurrence of potassic richterite in a mica nodule from the Wesselton kimberlite, South Africa. *Carnegie Institution of Washington, Yearbook* **68,** 320–324.

Erlank, A. J., Waters, F. G., Hawkesworth, S. E., Haggerty, H. L., Allsopp, R. S., Rickard, R. S. & Menzies, M., 1987. Evidence for mantle metasomatism in peridotite nodules from the Kimberley pipes, South Africa. In: Menzies, M. A. & Hawkesworth, M. C. (eds) *Mantle Metasomatism*. London: Academic Press, pp. 221–311.

Finger, L. W. & Burt, D. M., 1972. REACTION, a FORTRAN IV computer program to balance chemical reactions. *Carnegie Institution of Washington, Yearbook* **71,** 616–620.

Finnerty, A. A. & Boyd, F. R., 1987. Thermobarometry for garnet peridotite xenoliths. A basis for upper mantle stratigraphy. In: Nixon, P. H. (ed.) *Mantle Xenoliths*. New York: John Wiley, pp. 381–402.

Foley, S., 1991. High-pressure stability of the fluor- and hydroxy-endmembers of pargasite and K-richterite. *Geochimica et Cosmochimica Acta* **55,** 2689–2694.

Foley, S., 1992. Vein-plus-wall-rock melting mechanisms in the lithosphere and the origin of potassic alkaline magmas. *Lithos* **28,** 435–453.

Forbes, W. C. & Flower, M. F. J., 1974. Phase relations of titan-phlogopite, $K_2Mg_4TiAl_2Si_6O_{20}(OH)_4$: a refractory phase in the upper mantle? *Earth and Planetary Science Letters* **22,** 60–66.

Gilbert, M. C. & Briggs, D. F., 1974. Comparison of the stabilities of OH- and F-potassic richterites—a preliminary report. *Transactions, American Geophysical Union* **55,** 480–481.

Green, D. H., 1973. Experimental melting studies on a modal upper mantle composition at high pressure under water-saturated and water-undersaturated conditions. *Earth and Planetary Science Letters* **19,** 37–53.

Green, D. H. & Ringwood, A. E., 1967. The stability fields of aluminous pyroxene peridotite and garnet peridotite and their relevance in upper mantle structure. *Earth and Planetary Science Letters* **3,** 151–160.

Hall, A., 1982. The Pendennis peralkaline minette. *Mineralogical Magazine* **45,** 257–266.

Hariya, Y. & Terada, S., 1973. Stability of $richterite_{50}tremolite_{50}$ solid solution at high pressures and possible presence of sodium calcic amphibole under upper mantle conditions. *Earth and Planetary Science Letters* **18,** 72–76.

Harlow, G. E., 1994. High-*P* partitioning of K between Cpx and K-carbonate. *Transactions, American Geophysical Union* **75,** 369.

Harlow, G. E., 1995. K-amphibole and mica stability in K-rich environments at high *P* and *T*. *Transactions, American Geophysical Union* **76,** 298.

Harlow, G. E. & Veblen, B. R., 1991. Potassium in clinopyroxene: inclusions from diamonds. *Science* **251,** 652–655.

Harte, B., Hunter, R. H. & Kinny, P. D., 1993. Melt geometry, movement and crystallization, in relation to mantle dykes, veins and metasomatism. In: Cox, K. G., McKenzie, D. P. & White, R. S. (eds) *Melting and Melt Movement in the Earth*. Oxford: Oxford University Press, pp. 1–22.

Hawthorne, F. C., 1981. Crystal chemistry of the amphiboles. In: Veblen, D. R. (ed.) *Amphiboles and Other Hydrous Pyriboles—Mineralogy. Mineralogical Society of America, Reviews in Mineralogy* **9A,** 1–95.

Hawthorne, F. C., 1983. The crystal chemistry of the amphiboles. *Canadian Mineralogist* **21,** 173–480.

Heinrich, W., 1994. Potassium-fluor-richterite in metacherts from the Bufa del Diente contact-metamorphic aureole, NE-Mexico. *Mineralogy and Petrology* **50,** 259–270.

Helgeson, H. C., Delaney, J. M., Nesbitt, H. W. & Bird, D. K., 1978. Summary and critique of the thermodynamic properties of rock-forming minerals. *American Journal of Science* **278-A,** 229 pp.

Hinrichsen, Th. & Schürmann, K., 1977. Experimental investigation on the Na/K-substitution in edenites and pargasites. *Neues Jahrbuch für Mineralogie, Abhandlungen* **130,** 12–18.

Holland, T. J. B. & Powell, R., 1990. An enlarged and updated internally consistent thermodynamic dataset with uncertainties and correlations: the system K_2O–Na_2O–CaO–MgO–MnO–FeO–Fe_2O_3–Al_2O_3–TiO_2–SiO_2–C–H_2–O_2. *Journal of Metamorphic Geology* **8,** 89–124.

Huebner, S. J. & Papike, J. J., 1970. Synthesis and crystal chemistry of sodium–potassium richterite $(Na,K)NaCaMg_5Si_8O_{22}(OH,F)_2$: a model for amphiboles. *American Mineralogist* **55,** 1973–1992.

Hwang, P., Taylor, W. R., Rock, N. M. S. & Ramsay, R. R., 1994. Mineralogy, geochemistry and petrogenesis of the Metters Bore No. 1 lamproite pipe, Calwynyardah Field, West Kimberley Province, Western Australia. *Mineralogy and Petrology* **51,** 195–226.

Ionov, D. A. & Hofmann, A. W., 1995. Nb–Ta-rich mantle amphiboles and micas: implications for subduction-related metasomatic trace element fractionations. *Earth and Planetary Science Letters* **131,** 341–356.

Johannes, W., Chipman, D.W., Hays, J. F., Bell, P. M., Mao, H. K., Boettcher, A. L., Newton, R. C. & Seifert, F., 1971. An interlaboratory comparison of piston-cylinder pressure calibration using the albite breakdown reaction. *Contributions to Mineralogy and Petrology* **32,** 24–38.

Jones, A. P., Smith, J. V. & Dawson, J. B., 1982. Mantle metasomatism in 14 veined peridotites from the Bultfontein mine, South Africa. *Journal of Geology* **90,** 435–453.

Karzhavin, V. K., 1992. Thermodynamic parameters of amphiboles. *Geochemistry International* **29,** 63–71.

Kennedy, C. S. & Kennedy, G. C., 1976. The equilibrium boundary between graphite and diamond. *Journal of Geophysical Research* **81,** 2467–2470.

Konzett, J., Sweeney, R. J. & Compston, W., 1995. The correlation of kimberlite activity with mantle metasomatism. *Sixth International Kimberlite Conference, Extended Abstracts*. Novosibirsk: United Institute of Geology, Geophysics and Mineralogy, Siberian Branch of the Russian Academy of Sciences, pp. 285–286.

Kushiro, I. & Erlank, A. J., 1970. Stability of potassic richterite. *Carnegie Institution of Washington, Yearbook* **68,** 231–233.

Leake, B. E., 1978. Nomenclature of amphiboles. *American Mineralogist* **63,** 1023–1053.

Leung, I. S., Li, Y. L. & Han, Z. G., 1994. Metasomatised olivine, garnet and diopside entrapped in diamonds from Fuxian. *Transactions, American Geophysical Union* **75,** 192.

Luth, R. W., Trønnes, R. G. & Canil, D., 1993. Volatile phases in the Earth's mantle. In: Luth, R. W. (ed.) *Experiments at High Pressure and Applications to the Earth's Mantle. Mineralogical Association of Canada Short Course Handbook* **21,** 445–485.

Matsubara, S. & Motoyoshi, Y., 1985. Potassium pargasite from Einstödingen, Lützow–Holm Bay, East Antarctica. *Mineralogical Magazine* **49,** 703–707.

Mengel, K. & Green, D. H., 1989. Stability of amphibole and phlogopite in metasomatised peridotite under water-saturated and water-undersaturated conditions. In: Ross, J. (ed.) *Fourth International Kimberlite Conference. Australian Journal of Earth Sciences Special Publication* **14,** 571–581.

Merrill, R. B. & Wyllie, P. J., 1975. Kaersutite and kaersutite eclogite from Kakanui, New Zealand—water-excess and water-deficient melting to 30 kilobars. *Geological Society of America Bulletin* **86,** 555–570.

Meyer, H. O. A. & McCallum, M. E., 1986. Mineral inclusions in diamond from the Sloan Kimberlite, Colorado. *Journal of Geology* **94,** 600–612.

Millhollen, G. L., Irving, A. J. & Wyllie, P. J., 1974. Melting interval of peridotite with 5·7 percent water to 30 kilobars. *Journal of Geology* **82,** 575–587.

Mitchell, R.H., 1995*a*. Melting experiments on a sanidine phlogopite lamproite at 4–7 GPa and their bearing on the sources of lamproitic magmas. *Journal of Petrology* **36,** 1455–1474.

Mitchell, R. H., 1995*b*. *Kimberlites, Orangeites and Related Rocks*. New York: Plenum.

Mitchell, R. H. & Bergman, S. C., 1991. The geochemistry of lamproites. In: Mitchell, R. H. & Bergman, S. C. (eds) *Petrology of Lamproites*. New York: Plenum, pp. 295-351.

Modreski, P. J. & Boettcher, A. L., 1972. The stability of phlogopite + enstatite at high pressures: a model for micas in the interior of the Earth. *American Journal of Science* **272,** 852–869.

Mottana, A. & Griffin, W. L., 1986. Crystal chemistry of two coexisting K-richterites from St. Marcel (Val d'Aosta, Italy). *American Mineralogist* **71,** 1426–1433.

Mysen, B. O. & Boettcher, A. L., 1975. Melting of a hydrous mantle: I. Phase relations of a natural peridotite at high pressures and temperatures with controlled activities of water, carbon dioxide, and hydrogen. *Journal of Petrology* **16,** 520–548.

Mysen, B. O. & Boettcher, A. L., 1976. Melting of a hydrous mantle: III. Phase relations of garnet websterite + H_2O at high pressures and temperatures. *Journal of Petrology* **17,** 1–14.

Navon, O., Hutcheon, G. R., Rossman, G. R. & Wasserburg, G. J., 1988. Mantle-derived fluids in diamond micro-inclusions. *Nature* **335,** 784–789.

Nemec, D., 1988. The amphiboles of potassium-rich dykes of the southeastern border of the Bohemian Massif. *Canadian Mineralogist* **26,** 89–95.

Nixon, P. H. & Boyd, F. R., 1973. Petrogenesis of the granular and sheared ultrabasic nodule suite in kimberlites. In: Nixon, P. H. (ed.) *Lesotho Kimberlites*. Maseru: Lesotho National Development Corporation, pp. 48–56.

O'Reilly, S. Y., Griffin, W. L. & Ryan, C. G., 1991. Residence of trace elements in metasomatised spinel lherzolite xenoliths: a proton-microprobe study. *Contributions to Mineralogy and Petrology* **109,** 98–113.

Phillips, D. & Harris, J. W., 1995. Geothermobarometry of diamond inclusions from the DeBeers Pool Mines, Kimberley, South Africa. *Sixth International Kimberlite Conference, Extended Abstracts*, Novosibirsk: United Istitute of Geology, Geophysics and Mineralogy, Siberian Branch of the Russian Academy of Sciences, pp. 441–443.

Pollack, H. N. & Chapman, D. S., 1977. On the regional variation of heat flow, geotherms and lithospheric thickness. *Tectonophysics* **38,** 279–296.

Ringwood, A. E. & Major, A., 1971. Synthesis of majorite and other high pressure garnets and perovskites. *Earth and Planetary Science Letters* **12,** 411–418.

Robie, R. A., Hemingway, B. S. & Fisher, J. R., 1978. Thermodynamic properties of minerals and related substances at 298·15 K and 1 bar (10^5 Pascals) pressure and at higher temperatures. *US Geological Survey Bulletin* **1452**.

Ryabchikov, I. D. & Boettcher, A. L., 1980. Experimental evidence at high pressure for potassic metasomatism in the mantle of the Earth. *American Mineralogist* **65,** 915–919.

Schneider, M. E. & Eggler, D. H., 1986. Fluids in equilibrium with peridotite minerals: implications for mantle metasomatism. *Geochimica et Cosmochimica Acta* **50,** 711-724.

Schrauder, M. & Navon, O., 1994. Hydrous and carbonatitic mantle fluids in fibrous diamonds from Jwaneng, Botswana. *Geochimica et Cosmochimica Acta* **58,** 761–771.

Seifert, F. & Schreyer, W., 1971. Synthesis and stability of micas in the system K_2O–MgO–SiO_2–H_2O and their relations to phlogopite. *Contributions to Mineralogy and Petrology* **30,** 196–215.

Shannon, R. D., 1976. Revised effective ionic radii and systematic studies of interatomic distances in halides and chalcogenides. *Acta Crystallographica* **232,** 751–767.

Shimazaki, H., Michiaki, B. & Ozawa, T., 1984. Sadanagaite and magnesio-sadanagaite, new silica-poor members of calcic amphibole from Japan. *American Mineralogist* **69,** 465–471.

Sudo, A. & Tatsumi, Y., 1990. Phlogopite and K-amphibole in the upper mantle: implications for magma genesis in subduction zones. *Geophysical Research Letters* **17,** 29–32.

Susaki, J., Akaogi, M., Akimoto, S. & Shimomura, O., 1985. Garnet–perovskite transformation in $CaGeO_3$: in-situ X-ray measurements using synchrotron radiation. *Geophysical Research Letters* **12,** 729–732.

Sweeney, R. J., Thompson, A. B. & Ulmer, P., 1993. Phase relations of a natural MARID composition and implications for MARID genesis, lithospheric melting and mantle metasomatism. *Contributions to Mineralogy and Petrology* **115,** 225–241.

Tatsumi, Y. & Eggins, S., 1995. *Subduction Zone Magmatism*. Oxford: Blackwell Scientific Publications.

Tatsumi, Y., Murasaki, M., Arsadi, E. M. & Nohda, S., 1991. Geochemistry of Quaternary lavas from NE Sulawesi: transfer of subduction components into the mantle wedge. *Contributions to Mineralogy and Petrology* **107,** 137–149.

Taylor, W. R., Tompkins, L. A. & Haggerty, S. E., 1994. Comparative geochemistry of West African kimberlites: evidence for a micaceous kimberlite endmember of sublithospheric origin. *Geochimica et Cosmochimica Acta* **58,** 4017–4032.

Thompson, A. B., 1992. Water in the Earth's upper mantle. *Nature* **358,** 295–302.

Thompson, J. B., Jr, Laird, J. & Thompson, A. B., 1982. Reactions in amphibolite, greenschist and blueschist. *Journal of Petrology* **23,** 1–27.

Trønnes, R. G., Takahashi, E. & Scarfe, C. M., 1988. Stability of K-richterite and phlogopite to 14 GPa. *Transactions, American Geophysical Union* **69,** 1510–1511.

Van der Laan, S. R. & Foley, S. F., 1994. MARIDs and mantle metasomatism. *Mineralogical Magazine* **58A,** 505–506.

Velde, D., 1978. An aenigmatite–richterite–olivine trachyte from Puu Koae, West Maui, Hawaii. *American Mineralogist* **63,** 771–778.

Wagner, C., Deloule, E. & Mokhtari, A., 1995. Relations between MARID and PKP type mantle nodules from north Morocco: a mineralogical and hydrogen isotope study. *Terra Abstracts* **1,** 295.

Wagner, C., Deloule, E. & Mokhtari, A., 1996. Richterite-bearing peridotites and MARID-type inclusions in lavas from North Eastern Morocco: mineralogy and D/H isotopic studies. *Contributions to Mineralogy and Petrology* **124,** 406–421.

Walker, D., 1991. Lubrication, gasketing, and precision in multianvil experiments. *American Mineralogist* **76,** 1092–1100.

Walker, D., Carpenter, M. A. & Hitch, C. M., 1990. Some simplifications to multianvil devices for high pressure experiments. *American Mineralogist* **75,** 1020–1028.

Wallace, M. E. & Green, D. H., 1991. The effect of bulk rock composition on the stability of amphibole in the upper mantle: implications for solidus positions and mantle metasomatism. *Mineralogy and Petrology* **44,** 1–19.

Waters, F. G., 1987*a*. A suggested origin of MARID xenoliths in kimberlites by high pressure crystallization of an ultrapotassic rock such as lamproite. *Contributions to Mineralogy and Petrology* **95,** 523–533.

Waters, F. G., 1987*b*. A geochemical study of metasomatised peridotite and MARID nodules from the Kimberley pipes, South Africa. Ph.D. Thesis, University of Cape Town.

Waters, F. G. & Erlank, A. J., 1988. Assessment of the vertical extent and distribution of mantle metasomatism below Kimberley, South Africa. *Journal of Petrology, Special Lithosphere Issue*, 185–204.

Waters, F. G., Erlank, A. J. & Daniels, L. R. M., 1989. Contact relationship between MARID rock and metasomatised peridotite in a kimberlite xenolith. *Geochemical Journal* **23,** 11–17.

Yagi, T. & Akimoto, S.-I., 1976. Direct determination of coesite–stishovite transition by in-situ X-ray measurements. *Tectonophysics* **35,** 259–270.

Yagi, T., Akaogi, M. & Shimomura, O., 1987. In situ observation of the olivine–spinel phase transformation in Fe_2SiO_4 using synchrotron radiation. *Journal of Geophysical Research* **92,** 6207–6213.

Yoder, H. S., Jr & Kushiro, I., 1969. Melting of a hydrous phase: phlogopite. *American Journal of Science* **267-A**, 558–582.